FACULTY
OF MATHEMATICS
AND PHYSICS
Charles University

DOCTORAL THESIS

Marie Krátká

Electronic effects at the interface between biomolecules, cells and diamond

Supervisor of the doctoral thesis: doc. RNDr. Bohuslav Rezek, PhD.

Study programme: Biophycics, Chemical and Macromolecular Physics

Prague 2018

I declare that I carried out this doctoral thesis independently, and only with the cited sources, literature and other professional sources.

I understand that my work relates to the rights and obligations under the Act No. 121/2000 Coll., the Copyright Act, as amended, in particular the fact that the Charles University has the right to conclude a license agreement on the use of this work as a school work pursuant to Section 60 paragraph 1 of the Copyright Act.

In Prague 2018   Signature of the author:

Acknowledgements

Title:

Electronic effects at the interface between biomolecules, cells and diamond

Author:

Marie Krátká

Department / Institute:

Department of Biophysics, chemical and macromolecular physics, Faculty of Mathematics and Physics, Charles University in Prague

Research was conducted at:

Institute of Physics, Academy of Science of the Czech Republic, Department of Thin Films and Nanostructures, Cukrovarnická 10, 16200, Prague

Supervisor of the doctoral thesis:

doc. RNDr. Bohuslav Rezek, PhD., Institute of Physics, Academy of Sciences of the Czech Republic, v.v.i.

Keywords:
Field-effect transistors, diamond, proteins, cells

Abstract

Understanding and control of interactions between biological environment (cells, proteins, tissues, membranes, electrolytes, etc.) and solid-state surfaces is fundamental for biomedical applications such as bio-sensors, bio-electronics, tissue engineering and implant materials as well as for environmental monitoring, security and other fields. Diamond can provide unique combination of semiconducting, chemical, optical, biocompatible and other properties for this purpose.

In this thesis we characterize electronic properties of protein-diamond interface by employing a solution-gated field-effect transistor (SGFET) based on hydrogen-terminated diamond, surface of which is exposed to biological media. We elucidate the role of adsorbed protein layer on the electronic response of the diamond transistor. We investigate effects of cells (using mainly osteoblast cells as model) on diamond SGFETs transfer characteristics and gate currents. We employ nanocrystalline diamond (NCD) thin films of different grain sizes (80 - 250 nm) to characterize and discuss influence of grain boundaries and sp2 phase on bio-electronic function of SGFETs. We investigate effects of gamma irradiation on function and stability of hydrogen-terminated diamond SGFETs interfaced with proteins and cells, showing feasibility of real-time monitoring of radiation treatments. We developed and tested portable battery-driven device. We also show a way for recycling used diamond SGFET devices. The results may thus contribute to better understanding and novel applications of diamond SGFETs in biosensors and other fields.

Abstrakt

Pro biomedicínské aplikace, jako jsou biosenzory, bioelektronika, tkáňové inženýrství, optimalizace materiálů pro implantáty, monitorování životního prostředí atd., je zásadní interakce mezi biologickým prostředím (buňky, proteiny, tkáně, membrány, elektrolyty apod.) a povrchem pevné látky. Diamant může v tomto směru poskytnout unikátní kombinaci výborných polovodičových, mechanických, chemických, biokompatibilních a dalších vlastností.

V této dizertační práci charakterizujeme elektronické vlastnosti rozhraní protein-diamant pomocí polních tranzistorů na bázi diamantu zakončeného vodíkem, jehož hradlo je vystaveno biologickému médiu (SGFET). Objasňujeme roli adsorbované proteinové vrstvy na elektronickou odezvu diamantového tranzistoru. Zkoumáme vliv buněk (převážně osteoblastů jako modelových buněk) na převodní charakteristiky a na svodové proudy diamantových polních tranzistorů. Pro posouzení vlivu hranic zrn a sp2 fáze na bio-elektronickou funkci diamantových SGFETů jsme použili vrstvy nanokrystalického diamantu o různých velikostech zrn (80 nm – 250 nm). Studujeme vliv gamma záření na funkci a stabilitu diamantových polních tranzistorů s proteiny a buňkami, což může být užitečné pro monitorování biochemických procesů během radiační léčby. Vyvinuli a otestovali jsme přenosné zařízení pro měření tranzistorových charakteristik. Rovněž ukazujeme možnost recyklace použitých diamantových tranzistorů. Tyto výsledky mohou přispět k lepšímu porozumění a následným aplikacím diamantových SGFETů v biosenzorice a dalších odvětvích.

Table of Contents

1 Introduction

1.1 Biointerfaces of materials and bio-materials to proteins, cells, membranes

Understanding the interaction between the biological systems (cells, proteins, tissues, membranes, electrolytes etc.) and solid-state surfaces is essential for biomedical applications such as cell-based biosensors, bioelectronics, tissue engineering and the optimization of implant materials.

Cells, the cornerstones of living tissue, perceive their surroundings and subsequently modify it by producing extracellular matrix (ECM), which serves as a basis to simplify their adhesion, spreading and differentiation [1]. This process is considerably complex, flexible and strongly depends on the cell cultivation conditions including the type of the substrate. Surface roughness of the substrate, porosity and the wettability, the latter influencing protein conformation [2–4] of the substrate play an important role [4–8]. Materials which are commonly employed as substrates for in vitro testing are polystyrene and glass. In this context, diamond as a technological material can provide a relatively unique combination of electrical, optical and mechanical properties with chemical and biocompatible properties [9,10] and it is a perspective material for bioelectronic and electrochemical applications [11].

Diamond films can be employed as biosensors such as catalytic glucose sensors [12], capacitive sensors [13] or solution-gated field-effect transistors (SGFETs) [14,15].

1.1.1 Diamond as a bio-material

Diamond surface can be relatively easily further functionalized by organic molecules [16,17] and it is suitable for attachment of cells such as osteoblasts, fibroblasts, cervical carcinoma cells (HeLaG) [18,19] or cardiomyocyte cells [15]. Biological as well as electronic properties of intrinsic diamond can be significantly

altered by hydrogen and oxygen atomic surface termination which results in different properties such as electrical conductivity, electron affinity, and surface wettability. Oxygen terminated surfaces are hydrophilic and highly resistive while hydrogen terminated surfaces are hydrophobic and they induce p-type surface conductivity even on undoped diamond [20–22].

This enables the design of different types of electrical sensors. Solution-gated field-effect transistor is one possibility of these electrical sensors. In this thesis we focus on SGFET based on nanocrystalline diamond (NCD) films on glass employing surface conductivity of H-terminated diamond surface [14,23,24]. It is notable that diamond SGFET can operate without a gate oxide layer because the gate is insulated by hydrogen atoms hence it allows direct contact between biomolecules and the surface of SGFET channel [24,25] (see more details in Chapter 1.2). Therefore diamond SGFETs can be employed as cell biosensors for environmental monitoring, biomedicine research or other applications. Employing NCD SGFETs as cell biosensors requires understanding interaction between diamond, proteins and cells or other biomolecules as well as understanding effects of cell incubation process.

Diamond is also considered as a promising tissue equivalent material in radiation therapies due to its unique set of properties. Owing to high radiation hardness diamond is recognized as the most suitable material for radiation medicine where it can be used in one of three principal modalities — radiotherapy, radiation oncology or therapeutic radiology. The use of diamond in counters of radiation particles or gamma rays has been studied since the late 1940s [26]. For monitoring medical irradiations diamond offers an excellent tissue equivalence due to its atomic number ($Z = 6$) which is close to the human tissue ($Z_{muscle} = 7.42$) [27–30]. Most of the works have been focused on employing diamond in monitoring of radiation beams. However, little is still known about using diamond as biosensor for real-time monitoring of bio-chemical processes during radiation treatments. We investigate the influence of gamma irradiation on function and stability of planar diamond based solution-gated field-effect transistors.

1.1.2 FBS layer on diamond

Fetal bovine serum (FBS) is a significant component of the cell medium. Proteins from fetal bovine serum are essential for cell growth of diverse types of

cells, such as osteoblasts, fibroblasts, cervical carcinoma cells (HeLaG), and others in vitro. FBS contains crucial components for the cell growth (growth factors, hormones and cytokines). Without FBS in McCoy's 5A medium the cells can survive for few hours but will die during further cultivation [3,31]. Therefore we study its behavior on diamond. FBS is the most widely used growth supplement for the in vitro cell culture of eukaryotic cells. This is due to high content of embryonic growth promoting factors. It can be used in many different cell culture applications [14,19]. FBS comes from the blood drawn from a bovine fetus. Main protein component in FBS is a bovine serum albumin (BSA). BSA is a globular protein in dimension of 4 x 4 x 14 mm. Other specific proteins contained in FBS are vitronectin and fibronectin.

The FBS adsorption is done by immersing diamond into McCoy's 5A medium supplemented with 15% FBS. By optimized measurements of atomic force microscopy (AFM) topography in oscillating regime and by using advanced AFM regimes such as phase imaging, nanoshaving, and force spectroscopy we characterize FBS thickness, adhesion, conformation and selectivity on the H/O-diamond surfaces [3].
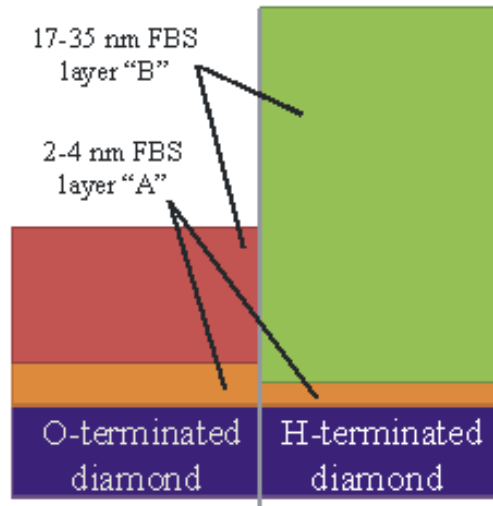
Figure 1.1: *Schematic model of FBS multilayer on diamond* [32].

A monolayer of proteins on diamond forms quickly after application (within 10 s) [32]. It has been shown by in situ atomic force microscopy that proteins assemble both on H-terminated (hydrophobic) and oxidized (hydrophilic) surfaces in a 2–4nm thin primary layer (Fig. 1.1) [3]. However, their conformation is different

and that controls selective cell adsorption and growth on H/O-micropatterns (Fig. 1.2) [14,19].
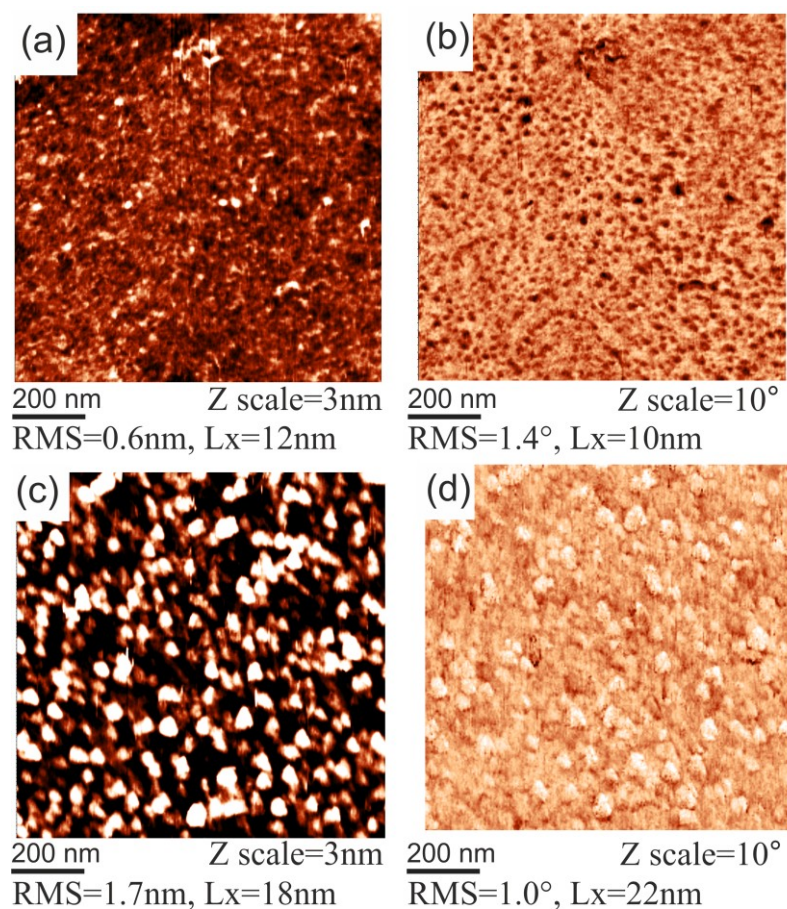
Figure 1.2: *AFM measurements in FBS/McCoy's medium on hydrogen- and oxygen terminated diamond surfaces with adsorbed FBS layers: topography and phase image on (a-b) FBS/H-terminated diamond and (c-d) FBS/O-terminated diamond [19].*

Thickness of protein layer on diamond is determined by nano-shaving procedure in atomic force microscope (Fig. 1.3).
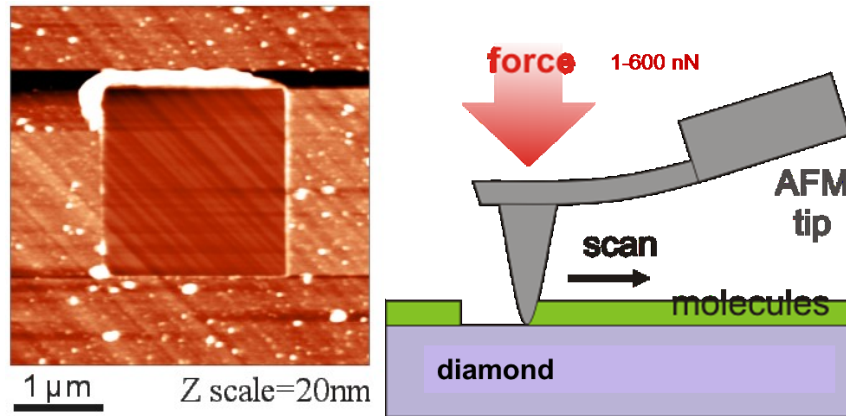
Figure 1.3: *AFM image of determination of protein layer thickness on diamond by nano-shaving procedure* [17].

1.1.3 Osteoblastic cells on diamond

For diamond-based biosensors, understanding interaction between cells and solid-state surfaces is essential. There are two main types of cells — eukaryotic (they have a true nucleus) and prokaryotic. Cells contain structures called organelles which carry out specific functions. The most important organelle in majority of plant and animals cell is nucleus which contains genetic information. Other organelles are mitochondria, plastids (such as chloroplasts), Golgi apparatus, endoplasmic reticulum etc. [33].

The cell membrane separates the interior of the cell from the outside environment. The cell membrane is selectively permeable to ions and organic molecules and controls the movement of substances in and out of cells. It consists of the lipid bilayer with embedded proteins. Membrane lipids are amphipathic molecules; they have a hydrophilic (polar) head group and hydrophobic (nonpolar) tails (Fig. 1.4). There are three major classes of membrane lipid molecules — phospholipids, cholesterol, and glycolipids [33].
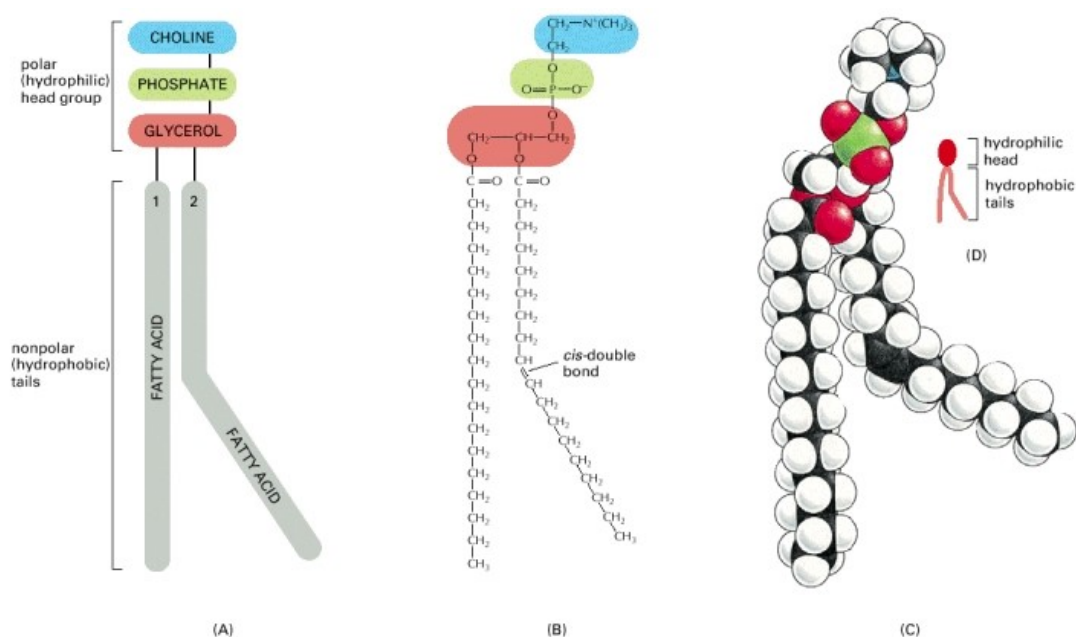
Figure 1.4: *The parts of a phospholipid molecule. This example is phosphatidylcholine, represented (A) schematically, (B) by a formula, (C) as a space-filling model, and (D) as a symbol. The kink resulting from the cis-double bond is exaggerated for emphasis. Taken from* [33].

In most experiments osteoblastic cells were used because SAOS-2 is a standard cell line, properties of which are stable even during long time period. This is why we can compare the results of different experiments, as well as our results with the literature. Nevertheless, other cells types as human fibroblasts, cervical carcinoma cells [19], HeLa cells [34], neurons [15,35] and non-adherent yeast cells [36] were plated on NCD or MCD samples for studying their behavior on diamond too.

Adhesion and morphology of cells were characterized by fluorescent staining of actin stress fibers (in green) and cell nuclei (in blue) using the protocol described in [37]. The staining was visualized using the E-400 epifluorescence microscope (Nikon); digital images were acquired with a DS-5M-U1 Color Digital Camera (Nikon) [38].

When the osteoblastic cells were plated and grown on the H-/O-terminated microstructures, they self-assembled preferably on the oxygen-terminated diamond surface. The cells' preference is independent of the width of the stripes between 30 and 200 μm (Fig. 1.5) [19] and of the surface roughness between 20 and 500 nm RMS (root-mean-square) [39].
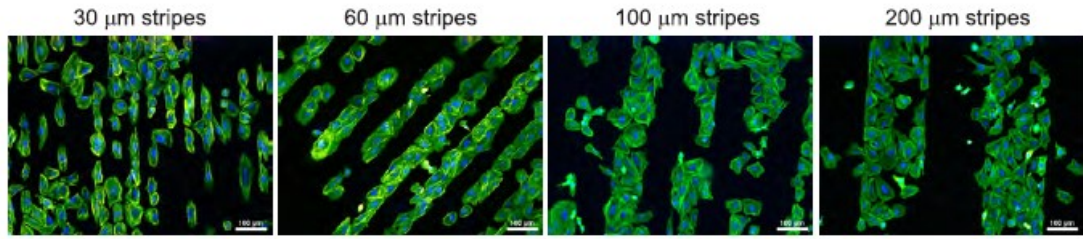
Figure 1.5: *Fluorescent microscopy images of osteoblastic cells (SAOS-2) cultivated for 2 days on H/O-terminated stripes of different widths (30 μm, 60 μm, 100 μm, and 200 μm) on diamond films. Initial cell seeding concentration was 2,500 cells/cm^2. The fluorescence shows actin stress fibers (green) and nuclei (blue). Scale bar is 100 μm* [19].

However, the shape of cells was found to be influenced by surface roughness [5,6] and the width of microstructures [18,19]. Cells grown on narrow O-stripes (30 μm, i.e. comparable with the size of the cell) are elongated and form chain-like structures. On the other hand, cells growing on wider stripes (60, 100 a 200 μm – larger than the typical cell size) spread over the whole width of the stripe. The H-/O-diamond boundary forms a sharp interface for cell adhesion [38].

Figure 1.6 shows the influence of cell seeding density (2,500 cells/cm^2 and 10,000 cells/cm^2). Cells plated at the higher density (10,000 cells/cm^2) colonize not only hydrophilic areas but also unfavorable hydrophobic regions. Fig. 1.6 (c) shows several cells that can bridge and colonize the hydrophobic area [19].

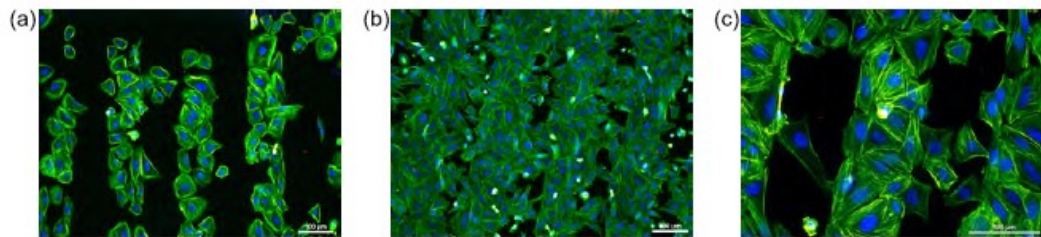**Figure 1.6:** *Fluorescent microscopy images of osteoblastic cells (SAOS-2) cultivated for 2 days on 100 μm H/O-terminated stripes on diamond films: (a) low initial cell seeding concentration (2,500 cells/cm^2), (b) high initial cell seeding concentration (10,000 cells/cm^2), and (c) cells bridging of unfavorable H-terminated regions. The fluorescence shows actin stress fibers (green) and nuclei (blue). Scale bar is 100 μm* [19].

The FBS serum is another factor which has impact on the selective growth of cells. Figure 1.7 demonstrates the influence of different initial FBS concentrations (0 and 15%) in the culture medium on the cell attachment onto the H/O-patterned surface. The range of serum concentrations 5-15% does not significantly affect the cell adhesion pattern (image for 15% FBS concentration is shown) [19].

Nevertheless, cells plated in a medium without FBS assemble of the surface independently of the surface termination. The cells' preference for a particular type of surface is thus presumably determined by the FBS proteins and not by a direct interaction between diamond surface dipoles and the cells. This is why the properties of FBS layers adsorbed on different types of diamond surfaces were investigated [38].
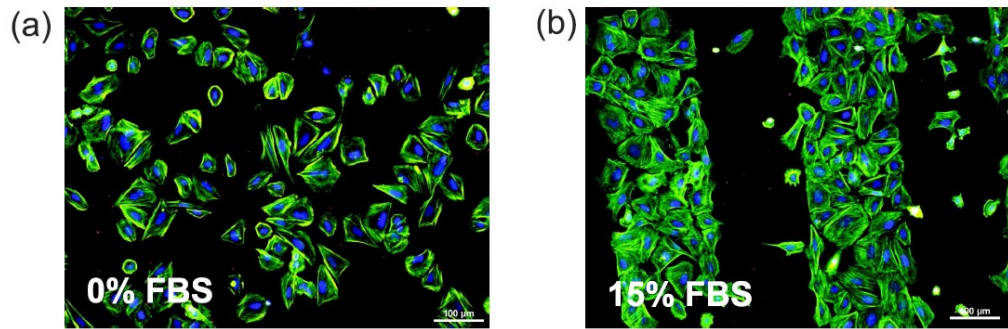
Figure 1.7: *Fluorescence images of osteoblasts, which were cultivated for 48 h on 100-µm-wide H-/O-diamond stripes with different starting concentrations of fetal bovine serum: (a) 0%, (a) 15%. Fluorescence microscopy shows actin filaments in green and cell nuclei in blue. In the 0% case, the cells were plated without the serum, however, the serum was added after 2 hours to allow cells to grow for next 48 h* [19].

1.2 Electrical Biosensors based on diamond

Diamond-based sensors are promising devices for bioelectrical applications due to biocompatibility, transparency, surface functionalization of diamond films, which allow real time electrical and optical monitoring of cell cultivation and/or cell functions. Diamond-based devices are fully transparent from UV to IR wavelengths. This feature enables both top- and back-side optical monitoring of cellular morphology and activity in real-time monitoring [13,40,41,42].

Diamond films can be employed as biosensors such as catalytic glucose sensors [12], capacitive sensors [13] or solution-gated field-effect transistors [14,15] taking advantage of diamond unique chemical and electronic properties [43].

1.2.1 Impendance biosensors

Impedance measurements seem to be one of the simplest and still a powerful method for monitoring of the cellular signals. As shown by many reports, the monitored impedance signal is sensitive not only to ionic currents but also to cell growth stages (i.e. cell attachment, spreading, shape, proliferation, differentiation and communication) [44–47].

The typical impedance sensors use gold interdigital electrodes (IDEs) which are deposited on an electrically insulating material (like glass or plastic). Up to now, several sensor systems were developed and they are commercially represented by xCELLigence system (Roche/Acea), ECIS - Electric Cell Substrate Impedance Sensing system (Applied BioPhysics), etc. Nevertheless, the use of gold electrodes restricts the available area for a direct optical monitoring of cultivated cells from the sensor backside. This limitation represents a disadvantage in specific experiments. Moreover, employing any surface biochemistry has to be optimized either to the used gold electrodes or to the carrying substrate. Finally, the sensor surface wettability is not simply controllable. One example of impedance sensor is the hydrogen terminated IDEs structures and it is shown in Fig. 1.8 [40,42].
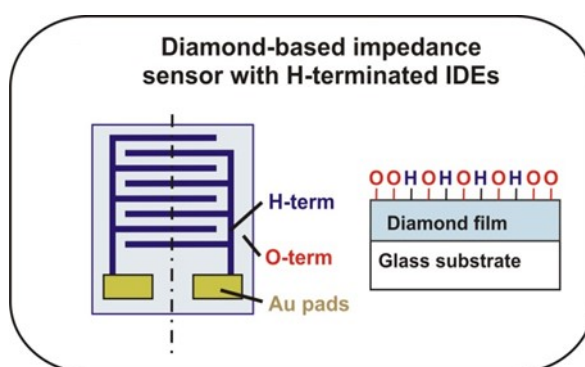

Figure 1.8: *Diamond based impedance sensor with H-terminated IDEs* [40].

The major drawback of capacitive sensing appears when it comes to miniaturization. In small dimensions the capacitance decreases significantly and the sensing becomes problematic. For miniature sensors, the solution-gated field-effect transistor (SGFET) design is more suitable as it can provide higher signal-to-noise ratio, good signal stability, its sensitivity can be increased, and can directly amplify the signal [14,24,48].

1.2.2 Diamond field-effect transistors

A field-effect transistor (FET) is an electric active element that uses an electric field to control the electrical behaviour of the device. It is also called unipolar transistor because FET uses either electrons (in n-channel FET) or holes (in p-channel FET) for conduction. The four main elements of the FET are named source, gate, drain, and a semiconducting body (substrate). The FET consists of an active channel through which electrons or holes flow from the source to the drain. Source and drain are connected to the semiconductor through ohmic contacts. The conductivity of the channel is a function of the potential applied across the gate and source terminals.

FETs can be made much smaller than bipolar transistor and due to their low power consumption and power dissipation makes them ideal for sensoric application.

Field-effect transistors exist in two major types: junction FET (JFET) and metal-oxide-semiconductor FET (MOSFET). JFET operates only in the depletion mode while MOSFET operates in both depletion mode and enhancement mode. Other difference between JFET and MOSFET is that JFET has less input impedance than MOSFET. We will concern with MOSFET because employed diamond FET is a MOSFET type. The gate of MOSFET is electrically insulated from the channel by the oxide layer (it is also called insulated-gate FET (IGFET)) [49–51].

The FET controls the flow of electrons (or holes) from the source to drain by affecting the size and shape of the space-charge region in the semiconducting body electrode by applying a negative or positive voltage to the gate. There are two types of MOSFET: MOSFET with induced channel (there is no conductive channel between source and drain; it creates only after applying the voltage to the gate) and MOSFET with conductive channel (permanent conductive channel exists between

source and drain; the Ids current flows even when the gate voltage is zero) (Fig. 1.9). Both types can exist with conductivity type *n* or *p* [49–51].

MOSFET with permanent channel works in depletion mode (decreasing the conductivity of the channel) and enhancement mode (increasing the conductivity of the channel).
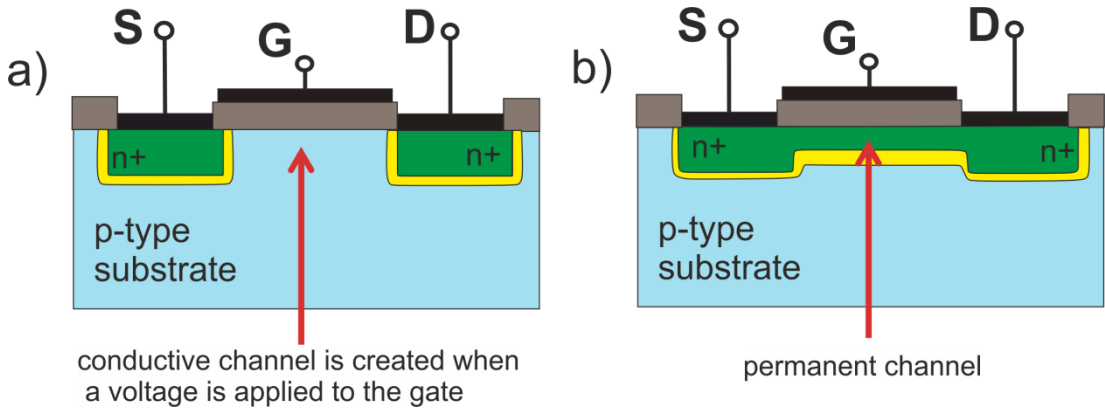
Figure 1.9: *MOSFET with induced channel (type n) (a) and MOSFET with conductive channel (type n) (b).*

MOSFET can operate in three regions:

1. Cut-off region: MOSFET is switched off (channel current Ids = 0). The gate voltage Ug is less than the threshold voltage Ut.
2. Linear region (ohmic mode): the channel is conducting and controlled by the gate voltage. Ug > Ut and the drain-source voltage Uds < Ug.
3. Saturation region (active mode): Ug > Ut and Uds > Ug – Ut. The drain current saturates. There is the lack of channel near the drain (pinch-off) [49,51,52].

Output characteristics symbolize dependence of the channel current Ids on the drain-source voltage Uds at constant gate voltage Ug. It is measured for different voltages Ug (Fig. 1.10b).

Equation of output characteristic in linear region is:

$$I_d = \mu_n C_{ox} \frac{W}{L} \left((U_g - U_t)U_{ds} - \frac{U_{ds}^2}{2} \right) \qquad (1.1)$$

where μ_n is the charge-carrier effective mobility, W is the gate width, L is the gate length and C_{ox} is the gate oxide capacitance per unit.

Equation of output characteristic in saturation region is:

$$I_d = \frac{\mu_n C_{ox}}{2} \frac{W}{L} \left(U_g - U_t\right)^2 \left(1 + \lambda(U_{ds} - U_{dsat})\right) \tag{1.2}$$

where λ is the channel-length modulation parameter [50,51,53].
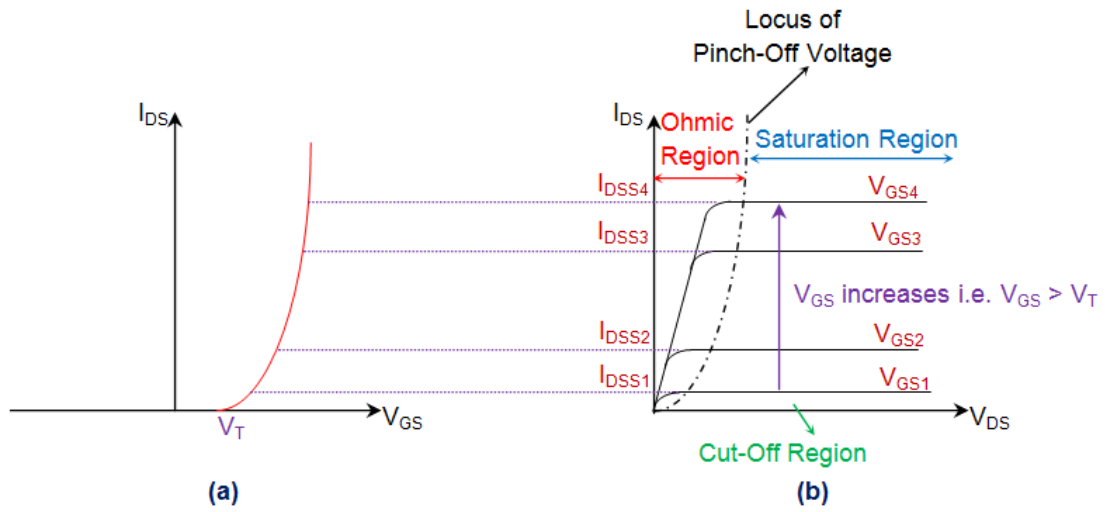
Figure 1.10: *Transfer characteristics (a) and output characteristics (b) of n-channel enhancement type of MOSFET. Taken from* [54].

Transfer characteristic means dependence of gate voltage Ug on the current Ids at constant voltage Uds (Fig. 1.10a).

The transconductance of the FET is defined as

$$g_m = \frac{\partial I_{ds}}{\partial U_g} \tag{1.3}$$

at constant Uds. In linear region:

$$g_{mL} = \frac{z \, \mu_n C_{ox}}{L} U_{ds} \tag{1.4}$$

and in saturation region transconductance is

$$g_{mS} = \frac{z \, \mu_n C_{ox}}{L} (U_{ds} - U_t). \tag{1.5}$$

Other FET parameter is the gain. The gain is defined as

$$gain = g_m \frac{U_{ds}}{I_{ds}} \quad [49–51,53].$$ (1.6)

Generally transistors enable miniaturization and direct transduction of signals in biosensing. This is indispensable for high density, high sensitivity, and high-speed sensors [55,56]. The main advantages of diamond SGFET in comparison to conventional silicon MOSFETs is excellent diamond biocompatibility and operation without a gate oxide layer because the gate is insulated by hydrogen atoms (in contrast to conventional Si/SiO_2 MOSFET-like devices) which enables much closer contact between biomolecules and the surface of channel. It can be also easily further functionalized by molecules such as DNA, where it can provide more stable and more efficient interface than other materials [15,16].

The diamond solution-gated FETs were at first used for pH [48,57] and DNA hybridization sensing [58]. Later on they were used for monitoring enzyme function and most recently for monitoring cell activity [15]. FETs based on monocrystalline diamond (MCD) [15,24,59] are employed more often in the fundamental studies than nanocrystalline diamond because MCD exhibits higher conductivity in comparison to nanocrystalline or polycrystalline diamond. On the other hand, NCD films are more likely to be widely applicable in bioelectronics as they are inexpensive in comparison to MCD and they can be easily fabricated from methane using microwave plasma on arbitrary substrates (silicon, glass [60], metals [61], plastic [62] and on large areas [63,64]. However, from the electronic point of view NCD is a complex system due to the presence of sp2 graphitic phase and grain boundaries [65].

The active gate area of NCD SGFET is realized by hydrogen-terminated diamond surface, which leads to p-type surface conductivity (see Fig. 2.17a). We use NCD SGFET as a cell biosensor to characterize (and amplify) electronic and biological effects at diamond interfaces. Functionality and properties of diamond SGFETs were characterized by electrical measurements in standard phosphate buffer saline solutions (PBS) at different pH. The gate voltage showed a linear dependence on the pH and the calculated sensitivity was approx. +19 mV/pH. This value is comparable with previously published values (approx. 15-17 mV/pH in such configuration) [15,34,36,66].

1.3 Aims of this work

Combining of semiconductor technology with organic materials represent a significant role for development of new nano- and bio-sensors as well as for other applications. Small dimensions allow high sensitivity, portability and wider availability of these devices. Electrical biosensor can be useful for detection of biological effects such as cellular properties, cell deaths etc. which could enable many applications in environmental monitoring, health care, tissue engineering, prosthesis etc.

This work aims at understanding and studying of fundamental phenomena at the interface between biomolecules, cells and diamond (effects of adsorbed protein layer and cultivated cells as well as effects of grain boundaries etc.). For these purpose SGFETs based on nanocrystalline diamond were developed where gate is functionalized by proteins or cells. It also aims to explore pathways for possible beneficial applications of these phenomena.

2 Experimental techniques

2.1 Fabrication of diamond layers and diamond SGFETs

2.1.1 Fabrication of diamond layers (CVD growth of diamond)

Nanocrystalline diamond films were grown on fused silica glass (UQG, 10x10x1 mm^3 size) by microwave plasma chemical vapor deposition (CVD) in Aixtron reactor using gas pressure 30 mbar, 1% CH_4 in H_2 and power 900–1000 W (Fig. 2.1). The deposition temperature was in the range of 550-600 °C. The periods of deposition were 1 h and 4.3 h to obtain different grain size and thickness. The surfaces of diamond films were hydrogenated in pure H plasma at 600 °C for 10 min. Before the deposition, the substrates were ultrasonically cleaned in isopropanol and deionized water (DIW) and were subsequently immersed for 40 min into an ultrasonic bath with a colloidal suspension of a diamond powder (UDD – ultra-dispersed diamond; NanoAmando, New Metals and Chemicals Corp. Ltd., Kyobashi) with nominal particle size of 5 nm. This process leads to the formation of a 5–25-nm-thin layer of nanodiamond powder. This nucleation procedure was followed by a microwave plasma-enhanced chemical vapor deposition (MWCVD) of diamond films [67,68].

This process ensures high quality of the hydrogen-terminated surface (surface conductance in the order of 10^{-7} S/sq) [69]. The surface morphology and chemical quality of NCD layers were characterized by AFM, scanning electron microscopy (SEM) and Raman spectroscopy. The grains exhibit clear facets that evidence their crystalline diamond form. Raman spectroscopy (excitation wavelength 325 nm) confirmed the diamond character of the layers [38].
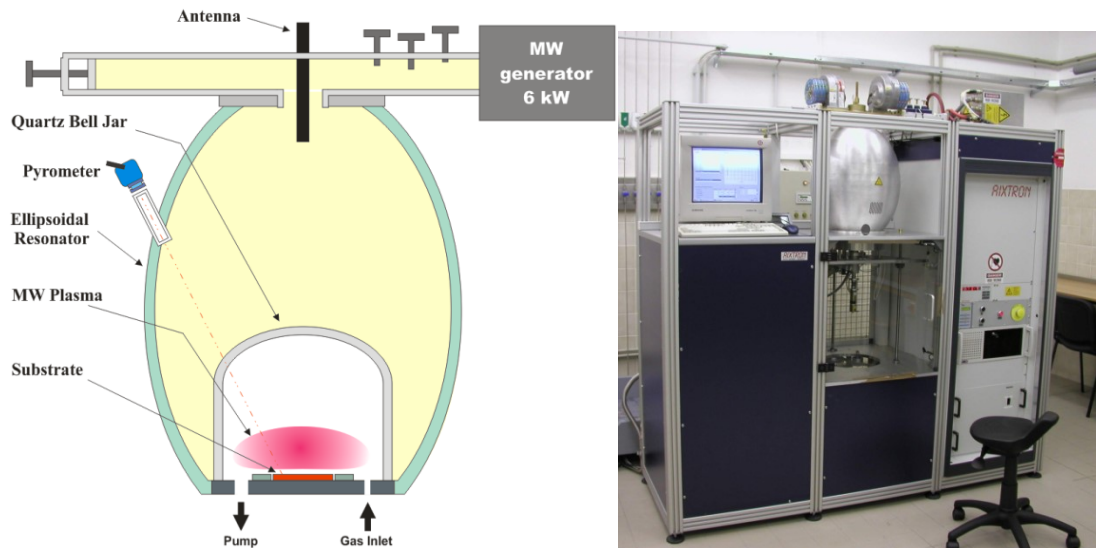
Figure 2.1: *Focused plasma reactor Aixtron P6 (plasma near sample)* [60].

2.1.2 Fabrication of planar SGFETs

Photolithographic masks were applied on H-terminated NCD films using positive ma-P 1215 photoresist (micro resist technology GmbH; 1.5 μm layer thickness) to define FET channels and contacts. The NCD films were treated in oxygen radio-frequency plasma (300 W, 3 min exposition time) to generate O-terminated areas which surround (and insulate) the channels connecting source and drain. Source and drain gold contacts were prepared by thermal evaporation (10 nm of Ti and 50 nm of Au) followed by lift-off technique. The samples were cleaned in acetone and photoresist stripper (remover mr-REM 660). The area between contacts was covered with positive photoresist ma-P 1240 (thickness 4 μm) and deep UV curing of resist for hardening and biocompatibility was applied. Photolithographic mask exposed openings of 60x60 μm^2 to define an active gate area (20 μm channel surrounded by 20 μm O-terminated areas in each side). Cross-sectional scheme of H-diamond SGFET fabrication process is shown in Figure 2.2. Top view scheme of the device after the step 8 in Figure 2.2 is shown in Figure 2.3 [67,68].
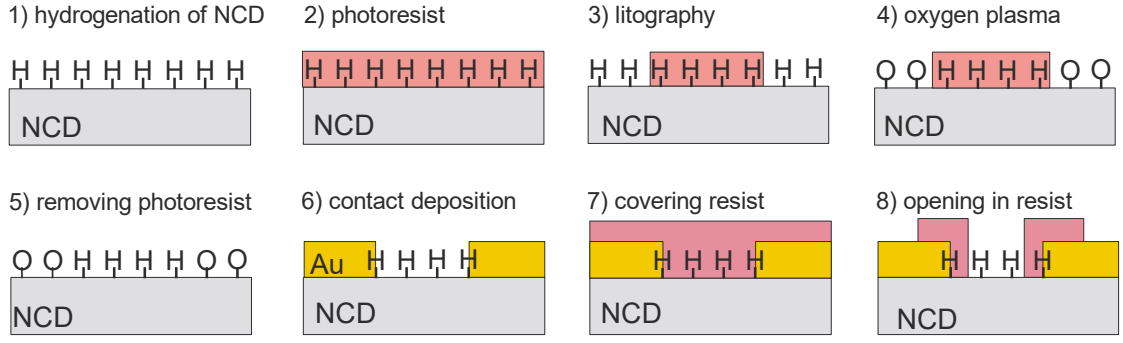
Figure 2.2: *Cross-sectional scheme of H-diamond SGFET fabrication process.*
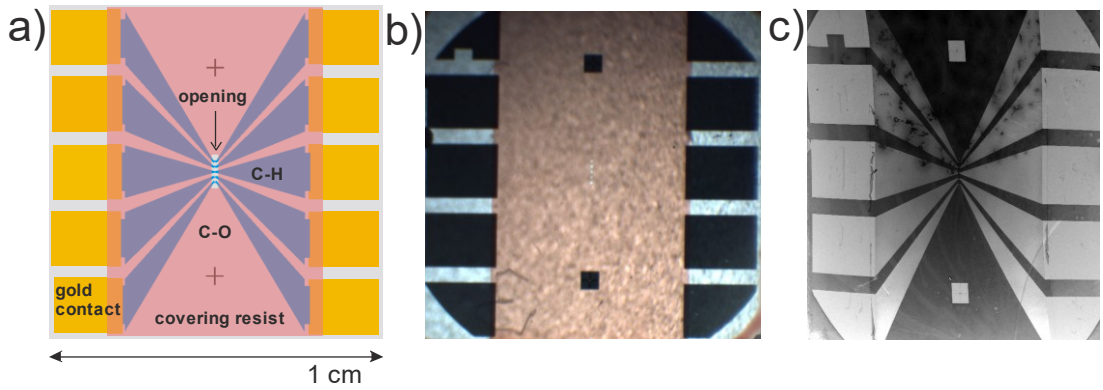
Figure 2.3: *Top view scheme (a), optical image (b) and SEM image (c) of NCD SGFET with 5 H-terminated channels.*

2.2 Fabrication of directly grown NCD FETs

2.2.1 Fabrication of directly grown NCD micro-channels

Direct growth of NCD channels was performed by microwave plasma chemical vapor deposition (CVD) on cleaned Si/SiO$_2$ substrates (10×10 mm^2, 1.5 μm thickness of SiO$_2$). Directly grown NCD FET channels were prepared by photolithographic processing with two polymer layers and by reactive ion etching (RIE) through photolithographic mask. The process is schematically shown in Fig. 2.4 and details can be found in the literature [70]. Briefly, Si/SiO$_2$ substrates were first covered with OFPR photoresist layer by spin-coating and dried at 100 °C (Fig.

2.4a). Then they were seeded with diamond nanoparticles applying an ultrasonic treatment (Fig. 2.4b). The seeding layer was covered by OFPR layer and dried (Fig. 2.4c). Thus diamond seeds are packed between two photosensitive layers (sandwich-like structure). This improves the pattern selectivity for diamond growth [70].

Microchannels were defined by photolithography patterning (Fig. 2.4d). Then, the reactive ion etching (CF_4/O_2 r.f. plasma parameters: 100 W, 150 mTorr, 3 min) was used as the final treatment step (Fig. 2.4e). Afterwards, growth of NCD thin films was performed in a focused microwave plasma CVD system (AIXTRON P6) from a methane/hydrogen gas mixture (Fig. 2.4f). Process parameters were as follows: microwave power 2.5 kW, 1% methane in hydrogen, total gas pressure 50 mbar, substrate temperature 800 °C, and total growth time 3 h. The surfaces of resulting three-dimensional diamond micro-structures were hydrogen-terminated in pure hydrogen plasma at 600 °C for 10 min in the same microwave apparatus [43].
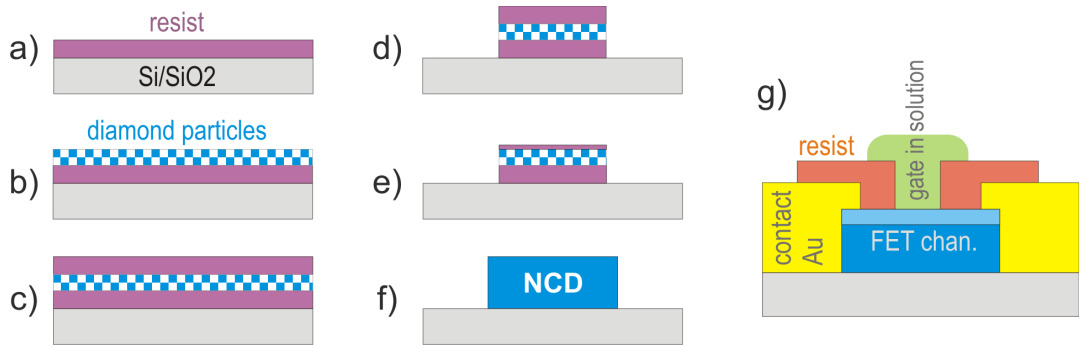
Figure 2.4: *Schematic illustration of the processing steps for fabrication of NCD micro-channels: coating with one layer of photoresist (a), seed layer formation (b), coating with second layer of photoresist (c), photolithography patterning (d) etching using RIE (e) and final growth of NCD micro-channel (f). Scheme of the complete solution-gate FET device with surface conductive, H-terminated diamond channel (g).*

2.2.2 Directly grown FET

For making complete FET device (see the scheme in Fig. 2.4 g), source and drain contacts were prepared by thermal evaporation (10 nm of Ti and 50 nm of Au) through lithographic masks followed by lift-off technique. The mask was removed in acetone and photoresist stripper (remover mr-REM 660). Then the area between contacts was covered with positive photoresists ma40 (4 μm). Other different types

of photoresists (positive photoresists OFPR with thickness 2–4 μm and negative photoresist SU8 3010 with thickness10 μm) were used for experiments concerning low temperature hydrogenation [43]. Deep UV curing of the photoresist for hardening and biocompatibility was applied on positive photoresists. Photolithographic mask exposed openings of 60×60 μm^2 to define an active gate area (20 μm channel surrounded by 20 μm substrates areas in each side). 5 μm channel was also prepared for some experiments (Fig. 2.6).
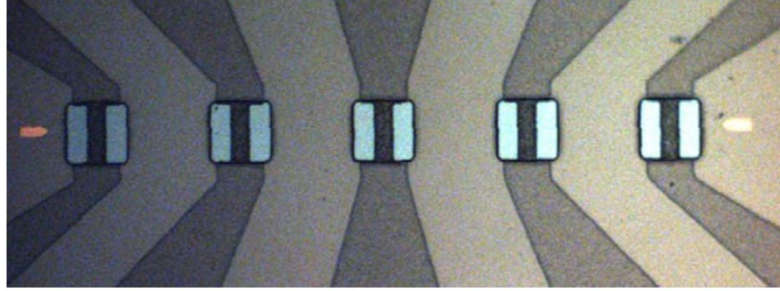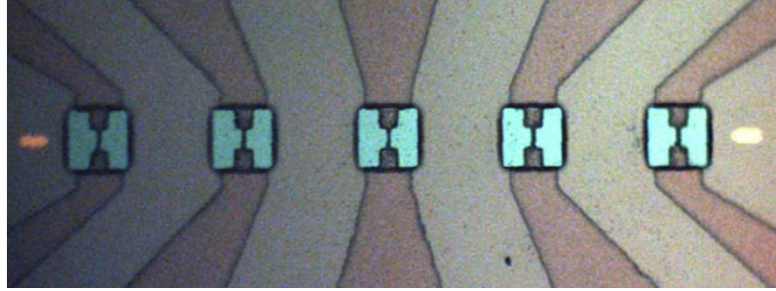
Figure 2.6: *Active area of directly grown FET with channel width: 20 μm and 5 μm.*

2.3 Material characterization

The structure and material composition of NCD films were studied by scanning electron microscopy (SEM), micro-Raman and atomic force microscopy (AFM).

2.3.1 Scanning Electron Microscopy

An electron microscope is an analogue of light microscope that uses a beam of accelerated electrons instead of photons as a source of illumination. Scanning electron microscope (SEM) creates images of a sample by scanning the surface with a focused beam of electrons. Resolution depends on the beam size and energy. SEM can achieve resolution better than 1 nanometer.

The main SEM components are source of electrons (gun), electromagnetic lenses, electron detector, sample chamber, computer and display to view the images (Fig. 2.7).
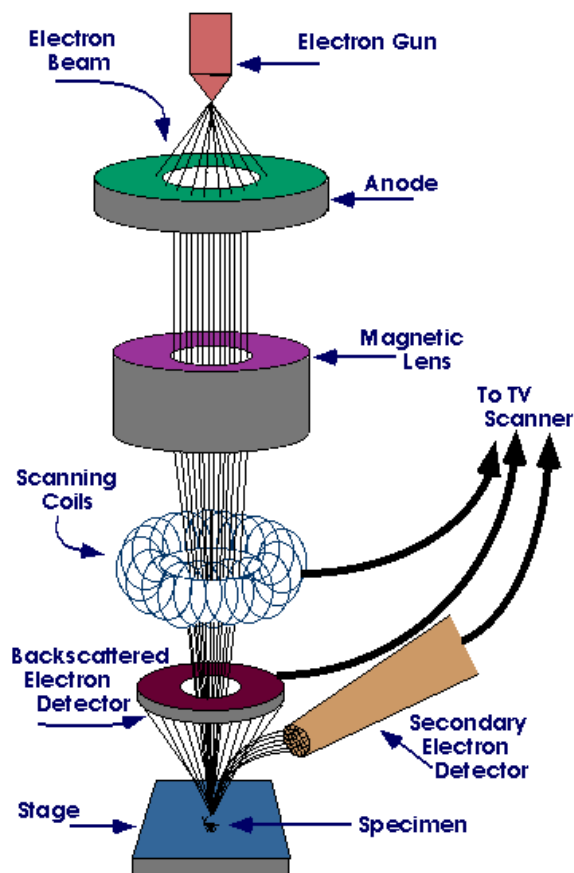
Figure 2.7: *The main SEM components. Taken from* [71].

Electrons are emitted from an electron gun (most often tungsten filament cathode placed in Wehnelt cylinder). Electrons are accelerated down toward sample by accelerating voltage (typically 0.1-30 kV). Then electrons pass through a combination of lenses and apertures to produce a focused beam of electrons which hits the surface of the sample. The electrons interact with atoms in the sample,

producing various signals that contain information about the surface topography and composition of sample. These signals are then detected by appropriate detectors. Interaction of electrons with material results in various signals including secondary electrons (SE), back-scattered electrons (BSE), characteristic X-rays and cathodoluminescence (CL), Auger electrons, absorbed current and transmitted electrons (Fig. 2.8) [72,73].
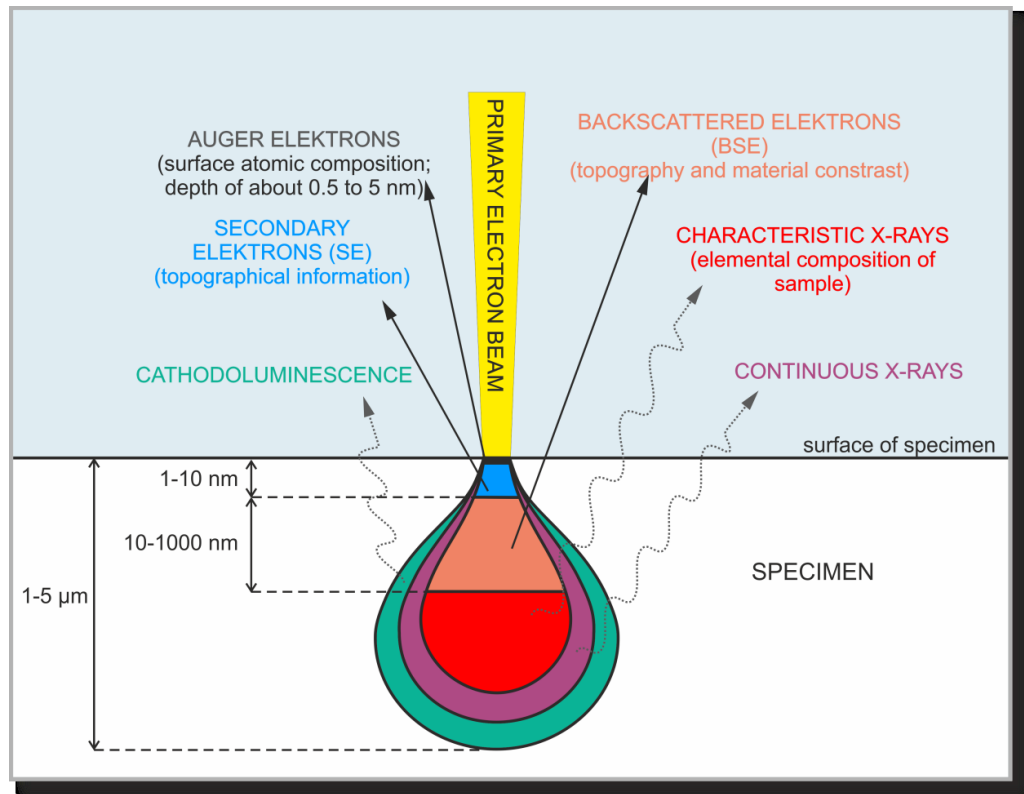
Figure 2.8: *Interaction between incident electrons and specimen.*

Secondary electron detectors are standard equipment in all SEMs and detection of SE is the most common type of detection in SEM. Secondary electrons are excited secondarily by electrons incident on the specimen. Since their generation region is as shallow as approx. 10 nm, the diffusion of incident electrons within the specimen has little influence on the image, thus allowing the best resolution to be obtained [72,73].

Figure 2.9 shows detailed surface morphology of NCD layers obtained from scanning electron microscope (the accelerating voltage was usually 10 kV, working

distance 8 mm). Average grain sizes used in our experiments are 250 ±50 nm and 80±50 nm [43,67].
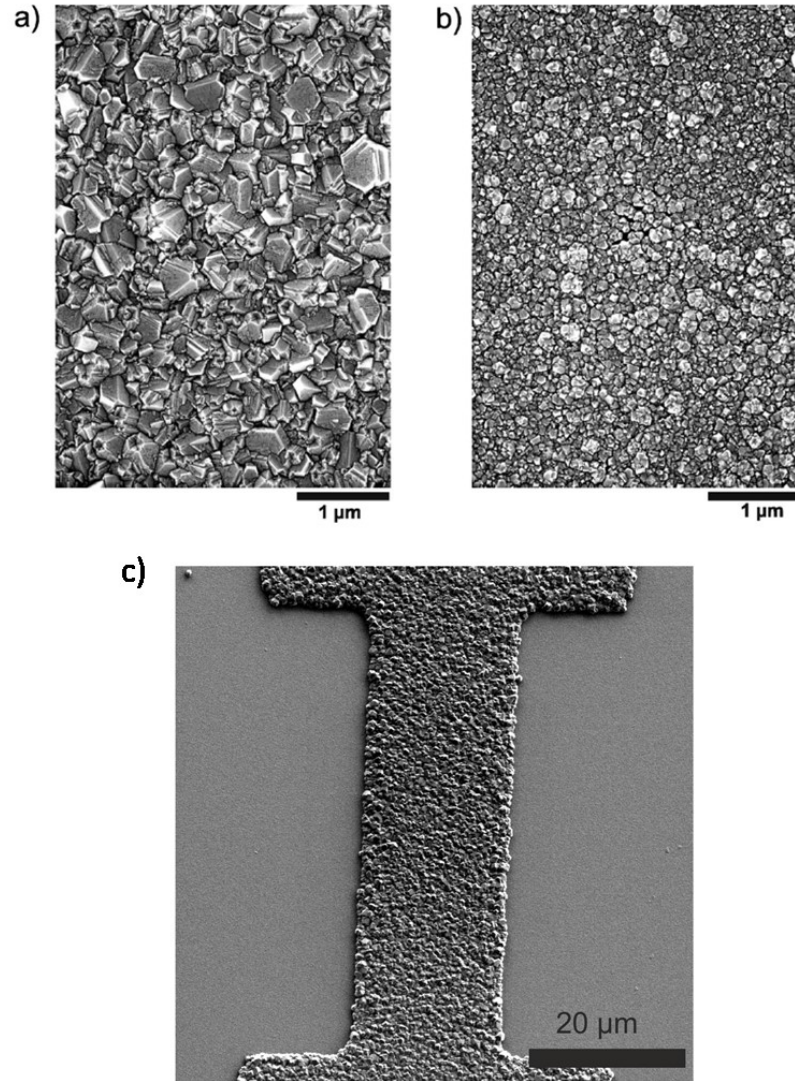
Figure 2.9: *Examples of SEM images of nanodiamond surface. NCD with average grain size of 250 nm (a) and 80 nm (b). SEM characterization of directly grown micro-channels (20 μm) (c).*

Grain size was estimated from the SEM images by a manual read-out of grain sizes across the SEM image and averaging of the data (Fig. 2.10).
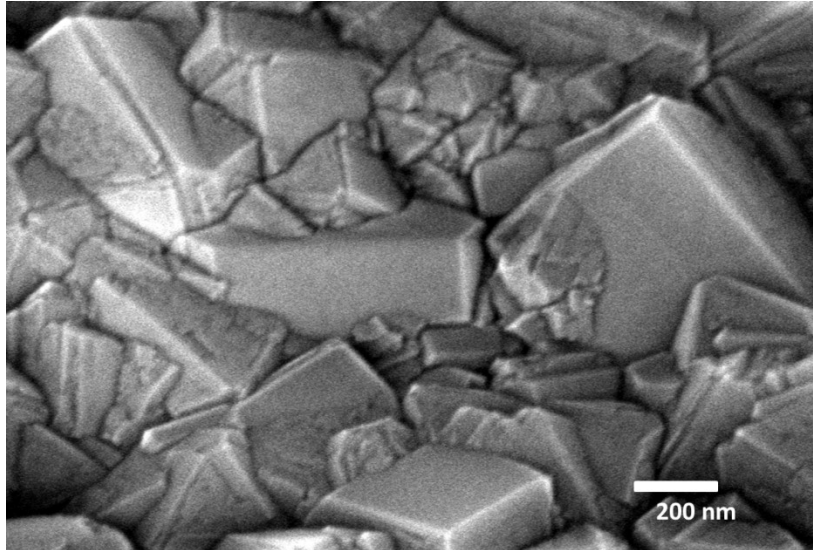
Figure 2.10: *Detailed SEM of directly grown NCD micro-channels.*

2.3.2 Raman spectroscopy

Raman spectroscopy is a method able to provide effective characterization of material composition from both surface and the bulk material. It is based on the scattering of electromagnetic radiation in material. There are two main types of scattering: elastic and inelastic.

In case of elastic scattering (Rayleigh scattering) the scattered photons have the same energy (frequency and wavelength) as the incident photons. Elastically scattered photons are the majority in light-induced excitation methods.

Nevertheless, there is also the small probability (about one in the 10^7) of a photon being inelastically scattered which represents the Raman effect. Raman effect belongs to the inelastic scattering of a photon by molecules which are excited to higher vibrational or rotational energy levels.

The Raman interaction leads to two different ways. As the incident photon interacts with a molecule, it excites it to a virtual state of higher energy. When it relaxes, the emitted photon has lower (Stokes) or higher (anti-Stokes) energy (fig. 2.11).

The spectrum of the inelastically scattered photons is named the Raman spectrum. It shows the intensity of the scattered light as a function of its frequency difference to the incident photons [74].
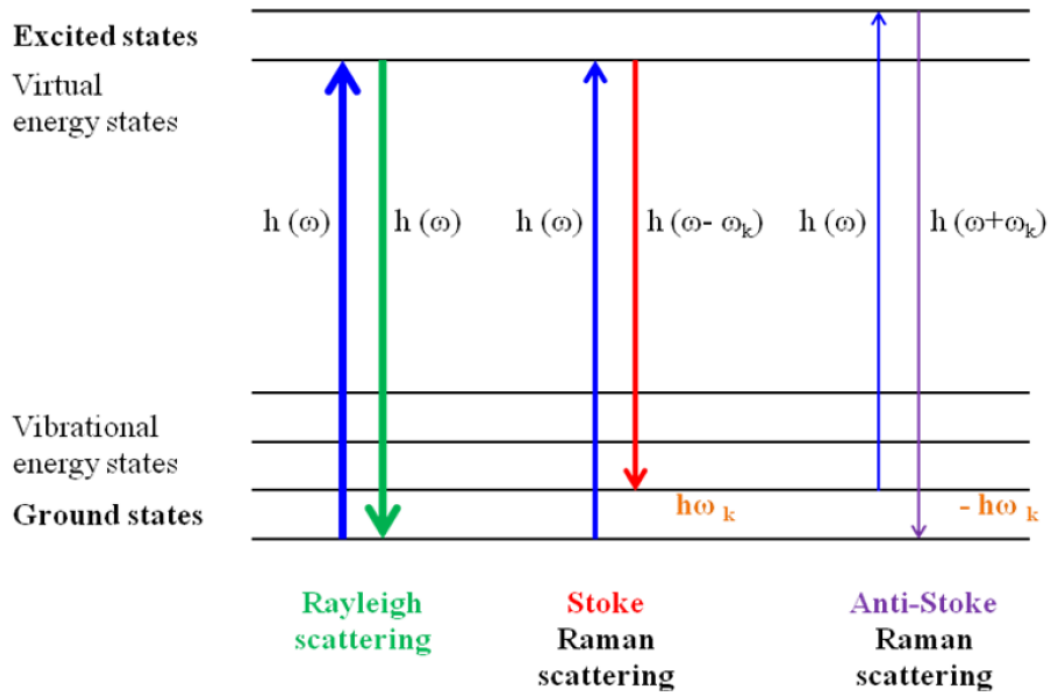
Figure 2.11: *Energy scheme of Rayleigh (elastic) and Raman (inelastic) scattering. For Raman, three types of scattering are possible: Rayleigh, Stoke Raman scattering and Anti-Stoke Raman scattering. Taken from* [75].

Raman spectroscopy is an appropriate technique for characterization of thin films because it is a fast, non-contact method and it is also safe for the samples (little or no sample preparation is required).

Pure diamond has a single sharp peak at 1332 cm^{-1} corresponding to the vibration of the sp3 diamond lattice. Amorphous carbon phase have two peaks. First peak is in the range of 1320 to 1360 cm^{-1}. It is labelled D band (disorder). The D band appears as a result of dislocations in the lattice. The second peak is in the range of 1500 to 1600 cm^{-1}. It is labelled G band (graphitic). The intensity of D band in proportion to the G band can be used to determine the degree of disorder in the sample. For study of NCD films excitation wavelength 325 nm was used. Raman spectrum shows clear diamond character of the films (Fig. 2.12). It reflects the presence of diamond phase (peak at 1332 cm^{-1}) and graphitic (sp2) phase (band at 1580 cm^{-1}) [76,77].
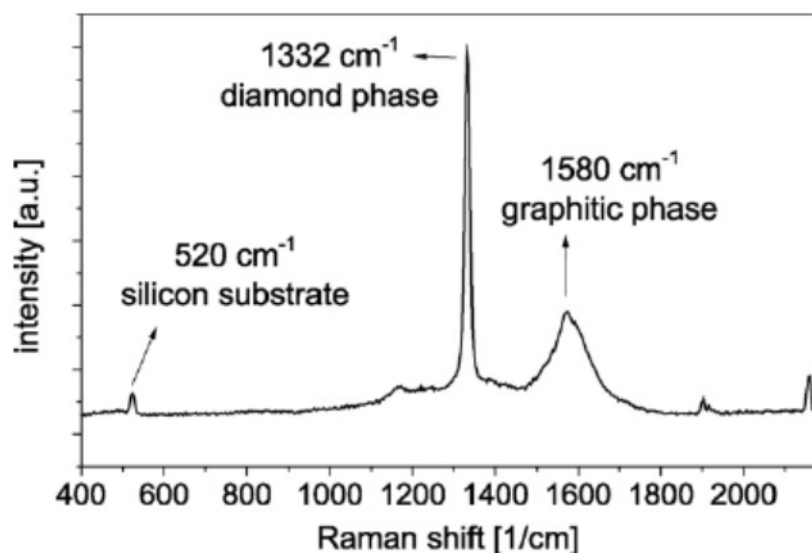
Figure 2.12: *Typical Raman spectrum of NCD films. Excitation wavelength was 325 nm* [14] .

2.3.3 Atomic Force Microscopy of FETs and proteins on diamond

Atomic Force Microscopy (AFM) is a microscopic technique using for 3D screening of surfaces. AFM is one of technique of scanning probe microscopy (SPM). The AFM consist of a cantilever with a sharp probe and it is based on detection forces between probe and the sample surface. When the probe is brought into proximity of a sample surface, forces between the probe and the sample lead to a deflection of the cantilever. There are several types of short-range and long-range interactions. The most important of these interactions are Van der Waals interaction and ionic repulsion (Fig. 2.13). There are three basic modes of operation in AFM: contact, non-contact and tapping (Fig. 2.14).
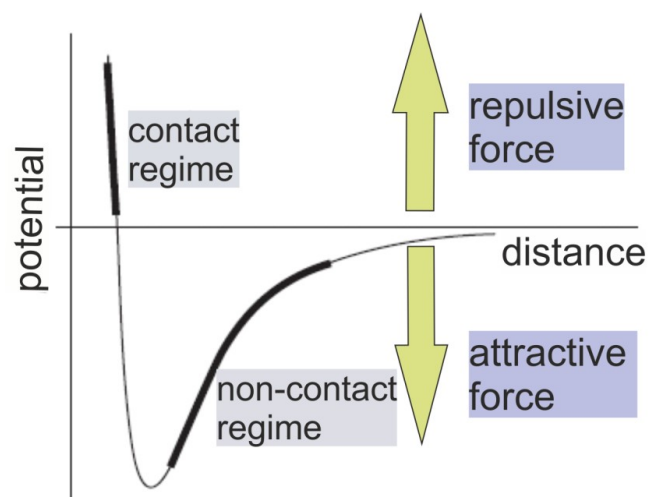
Figure 2.13: *The effect of tip-to-sample distance on the force interaction between tip and sample. Adapted from* [78].

Figure 2.14: *Three basic modes of operation in AFM: a) contact, b) non-contact and c) tapping. Adapted from* [78].

AFM study of protein layer

Study of protein layer was performed using AFM on monocrystalline diamond. In AFM experiments polished MCD substrates with RMS roughness < 1 nm were used instead of NCD substrates with RMS roughness > 10 nm. Low substrate roughness is required for such measurements because the thickness of protein layer is around 2–4 nm. Moreover, it is hard to detect FBS layer on NCD by AFM due to high tip wear during AFM nanoshaving. For those measurements the Ntegra AFM (NT-MDT) with Multi75Al cantilevers (Budget sensors) was used. To analyze AFM results Nova (NT-MDT) and Gwyddion software were used.

AFM study of protein layer was also used in low temperature hydrogenation experiments. To check the effectiveness of low temperature hydrogen termination, FBS was adsorbed on the surface of MCD from 15%

FBS solution for 10 min. Then the sample was cleaned with water and dried by air flow. The thickness of the protein layer was measured in air using AFM nanoshaving method [17,19,32]. Then the low temperature hydrogen termination at 200 °C was performed and the protein thickness was again measured using the same method [43] (see Fig. 3.15).

Besides proteins, we use AFM to study of NCD films. Fig. 2.15 shows three-dimensional AFM topography across a scratch in NCD films with different grain sizes.
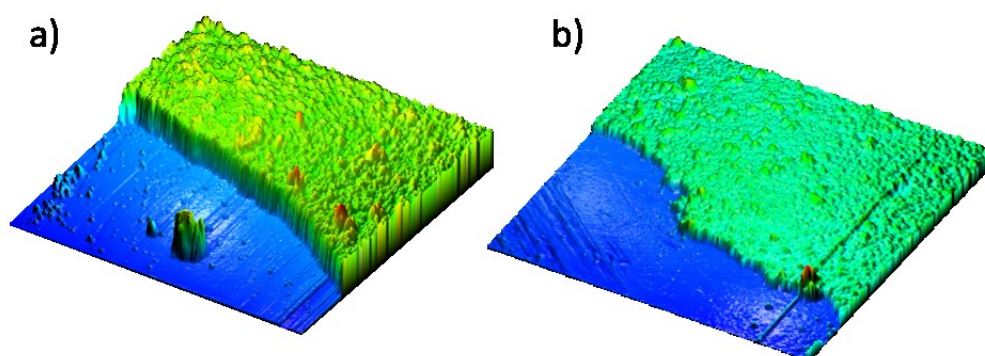
Figure 2.15: *Three- dimensional AFM topography across a scratch in NCD films. Thickness of NCD layer is 445 nm (a) and 108 nm (b). Scan dimensions are 20 μm x20μm in both cases.*

2.4 Transistor characteristics setup

Gating of SGFET was realized by immersing H-terminated channel into electrolyte solutions which were in contact with Ag/AgCl gate electrode (Fig. 2.16). Types of used solutions were: (1) McCoy's 5A medium (BioConcept), (2) McCoy's 5A medium supplemented with heat inactivated 15% fetal bovine serum (FBS; Biowest), (3) McCoy's 5A medium with 15% FBS and HEPES buffer, (4) HEPES buffer, and (5) Britton–Robinson buffer (pH 7). HEPES (4- (2-hydroxyethyl)-1piperazineethanesulfonic acid) is a zwitterionic organic compound used in buffer

solutions. McCoy's 5A medium is a general purpose cell cultivation medium used to support many types of primary cells and cell lines. It was prepared by Dr. Thomas McCoy by modification of Basal Medium 5A [67].
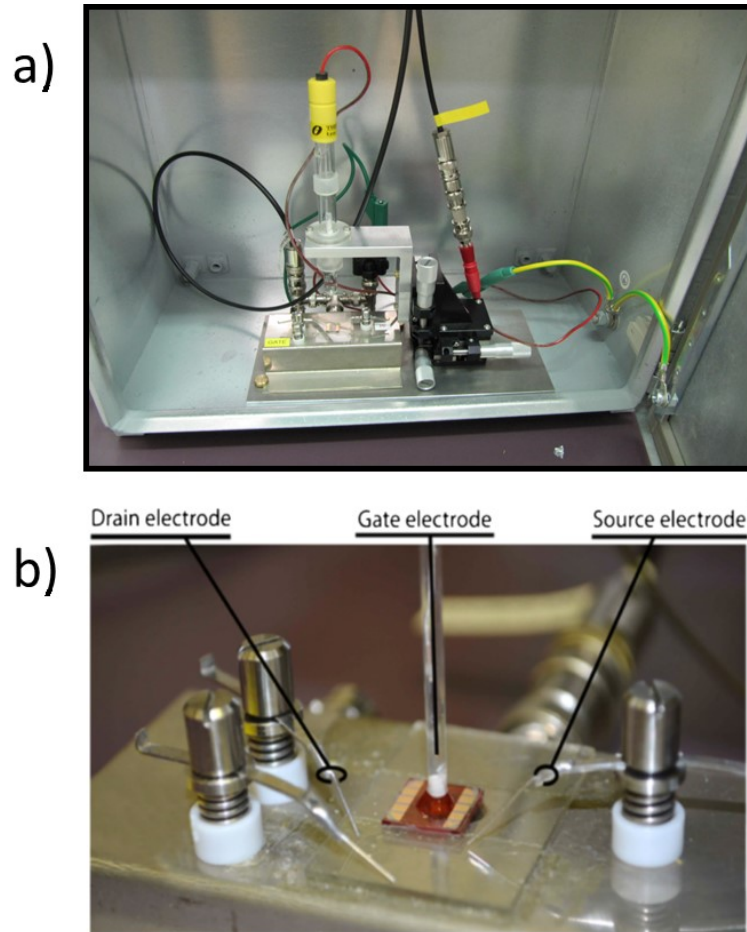
Figure 2.16: *Bio-FET setup image (a) and detail (b)* [36] .

The transistor output, transfer, and temporal characteristics were measured using Keithley K327 source-measure units at Faraday cage and using custom software package. The software was made using a measurement and control software package developed under Delphi by A. Fejfar, Institute of Physics. We show the third characteristics which are stabilized in short-term. The sweeping rate was 50 mV/s and initial delay time was 5 s. All experiments were performed at room temperature. As for incubation experiments with or without cells, all FETs were

stored in an incubator at 37 ºC, only during measurements they were kept at room temperature.

In short term (under which the FET measurements are conducted) such conditions are not detrimental to cells or to other solutions we have used. Temperature difference between room temperature and temperature of 37ºC does not influence the stability of the device (generally, our devices are stable at least up to 100 ºC) [67,68,79].

Fig. 2.17 shows schematic drawing of solution-gated field-effect transistor (SGFET) based on surface conductivity of H-terminated diamond.
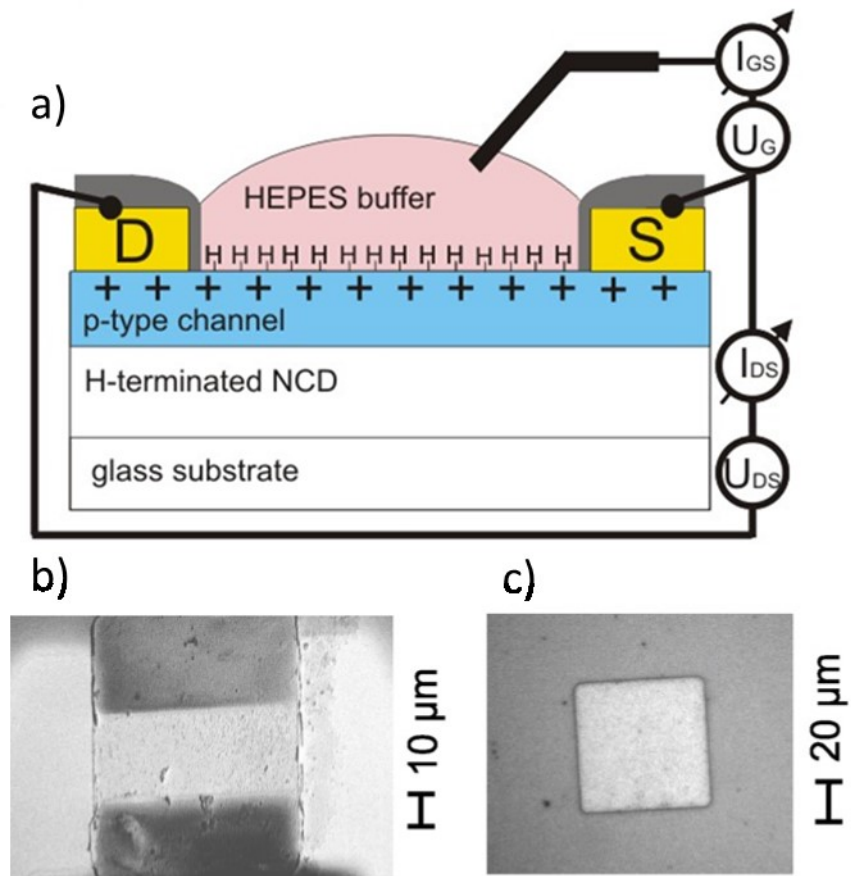
Figure 2.17: *(a) Schematic drawing of solution-gated field-effect transistor (SGFET) based on surface conductivity of H-terminated diamond. The gate is insulated by H atoms. The proteins and cells in the medium are thus interfaced directly with the diamond surface. (b) Electron microscopy image of the in-plane H-terminated channel (bright) surrounded by oxidized insulating surface (dark). (c) Optical microscopy image (bright field, 20× objective) of the device active area showing opening in the encapsulation. The channel structure cannot be seen as diamond is flat and optically transparent.*

2.5 Low temperature hydrogenation setup

Commonly used relatively high substrate temperatures (T ≥ 600 °C) during diamond growth and hydrogenation lead to partial or complete damage of the metal electrodes or other electronic parts [80]. Thus, 3D transistors including the encapsulation (resist OFPR, ma40, SU8 3010), gold contacts and with adsorbed proteins on diamond surface were exposed to hydrogen plasma using low temperature in two microwave plasma reactors (focused plasma reactor and linear plasma reactor). Fig. 2.18 shows a schematic drawing of fundamental differences between these two reactor setups. The main advantage of low temperature hydrogenation (LTH) in linear plasma reactor is a larger distance (7 cm) between the high-density plasma region and the sample surface [64,81]. Hydrogen termination at 200 °C performed in linear antenna plasma system is efficient to induce hydrogen-terminated conductive surfaces. No damage of polymer-based passivating layer (SU8) as well as Au contacts was observed [81]. In our case samples were exposed to linear hydrogen plasma at the following conditions: microwave power 1000 W, vacuum pressure 0.3 mbar, 100 sccm of hydrogen flow, and processing time 30 min. The substrate temperature was in the range of 200 – 300 °C with the accuracy of ±10°C.

The parameters of LTH in focused plasma were as follows: microwave power 800–1500 W, vacuum pressure 20–30 mbar, hydrogen flow 300 sccm, temperature 300 °C (the lowest achievable), processing time 20 min [43].
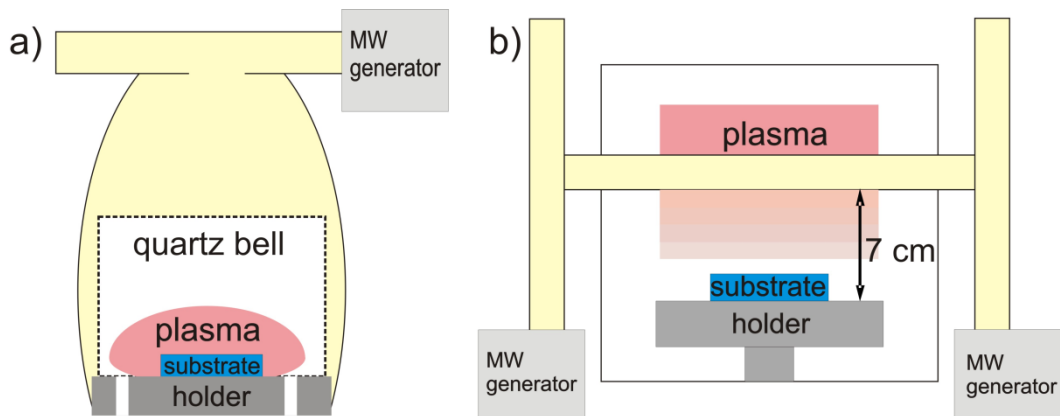
Figure 2.18: *Schematic drawing of microwave CVD reactors: focused plasma reactor (a) and linear antenna reactor (b). Position of the substrate with respect to the plasma is indicated.*

2.6 FBS adsorption

For understanding of effects at the interface between diamond and the biological system it is necessary to resolve influence of protein layer on NCD SGFET characteristics.

Proteins were adsorbed on the active area of diamond SGFET from 5 μl droplet of 15% FBS solution (Biowest) in McCoy´s 5A medium (BioConcept) (Fig. 2.19). A monolayer of proteins on diamond forms quickly after application [3]. There is no rinsing applied and SGFET characterizations directly follow as described further below [14].
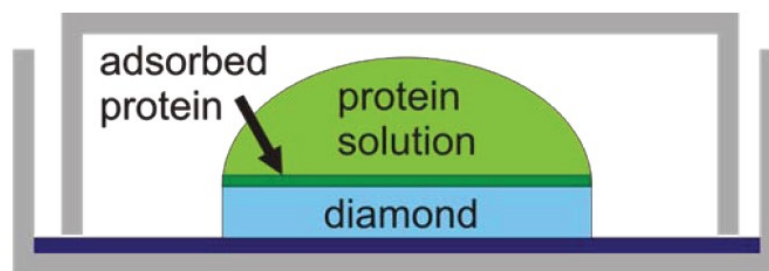
Figure 2.19: *Adsorption of proteins from FBS solution on NCD.*

2.7 Cell cultivation, including radiation setup

Human osteoblast-like SAOS-2 cells (sarcoma osteogenic, DSMZ GmbH) were grown in the McCoy´s 5A medium (BioConcept) supplemented with heat inactivated 15% FBS (Biowest), penicillin (20 U/ml) and streptomycin (20μg/ml). Hepes was added to the medium because of the absence of CO_2 atmosphere during the measurement. Sterilization prior to cell plating was performed by UV-C for 10 min. We use a standard germicidal low-pressure mercury lamp (TUV 15W/G15 T8, Philips) which emits UV-C radiation with the peak at 253.7 nm. Power is 15 W. Sample distance from lamp is 20 cm.

Cells were plated in the densities of about 10,000 cells/cm^2 using a droplet technique: substrate surface was covered by 10 μl droplet of cell suspension in the appropriately supplemented medium. At low initial cell concentrations (2500 cells/cm^2) the cell may selectively arrange only on oxidized part of surface. High cell concentrations (>10,000 cells/cm^2) ensure that the whole surface will be colonized by the cells during cultivation [19]. After 1 h incubation 1.4 ml of medium supplemented with 15% FBS was added and cells cultivated for 2 days in 5% CO_2 at 37 ºC. Stable 5% CO_2 concentration in the atmosphere during the cell cultivation helps the bicarbonate buffer in cultivation media to sustain the optimal pH (7.1–7.4). We characterized the effects of exposure to HEPES buffer and McCoy's cell medium with fetal bovine serum (FBS) proteins, rinsing by phosphate buffered saline (PBS), UV sterilization, and cell culturing process with or without cells on the SGFET transfer characteristics in HEPES buffer solution. Cells were let to delaminate and were washed by PBS and DIW [14,67].

Fig. 2.20 shows optical image of the active device area with incubated SAOS-2 cells.
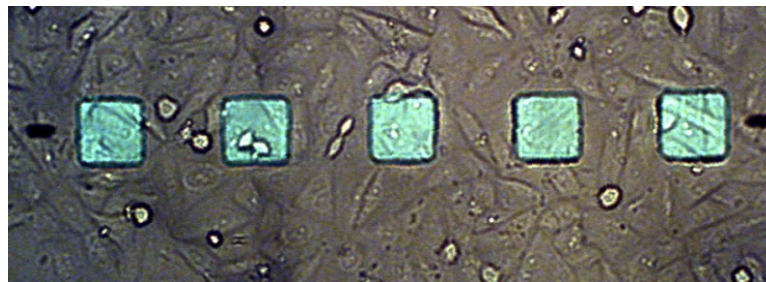
Figure 2.20: *Optical image of the active device area with incubated SAOS-2 cells (width of window is 60 μm).*

Gamma irradiation procedure

Blank SGFETs, SGFETs with adsorbed FBS and SGFETs with cells were irradiated by up to (5 ± 0.05) Gy of gamma radiation (Chisostat, Chirana, ^{60}Co source, dose rate of 6 Gy/min at the sample position). The irradiation of samples with proteins and FETs with cells was performed at Department of Radiation Dosimetry at Nuclear Physics Institute of the Czech Academy of Sciences (in collaboration with Dr. Marie Davídková). The uncertainty in dose can come from uncertainty of exposure time (determined uncertainty below 1%) and sample position (incorrect sample positioning of 1 mm from defined position corresponds to dose change of 1%). The dose of 5 Gy was used as it corresponds to about 10% survival of human fetal osteoblasts in vitro [82] and it is similar to typical therapeutic doses. During the irradiation, the SGFETs were inserted upright into plastic bottles filled with cell medium used for preceding cell cultivation. The diamond surface was faced to the gamma radiation source. A schematic drawing of the experimental setup during the irradiation is shown in Fig. 2.21. AFM measurements confirmed that proteins were adsorbed on monocrystalline diamonds which were then irradiated in the same configuration. The irradiation dose was up to (300±3) Gy in this case in order to corroborate the observed trends [83].
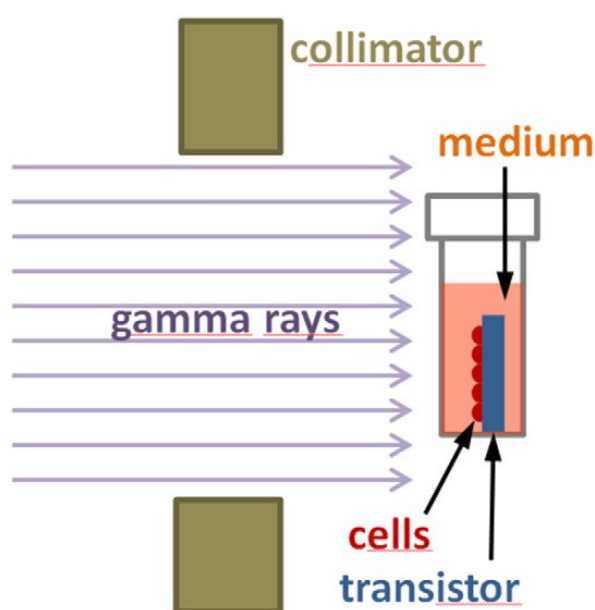
Figure 2.21: *Schematic drawing of the experimental setup during gamma irradiation experiments.*

3 Results and Discussion

3.1 Thin film NCD SGFET basic characteristics

We studied solution-gated FETs based on H-terminated nanocrystalline diamond films exhibiting surface conductivity and we showed that NCD with grain sizes down to 80 nm and film thickness of 100 nm prepared by focused plasma process as well as very thin NCD films growth by linear antenna microwave plasma CVD process are fully operational as SGFET and can serve as transducers (and partly also as amplifiers) of biological and/or environmental characteristics to electrical signals.

The example of output, transfer and gate current characteristics of pristine SGFET device measured in HEPES buffer solution (pH 7.14) is presented in Figure 3.1. The output characteristics were measured at gate voltages from 0.6 V to −0.6 V. They prove transistor character of the NCD SGFETs. They show typical increase and saturation of the channel current as a function of drain-source voltage as well as modulation by gate voltage Ug. The channels can be closed at Ug = 0.2 V. The channel current of SGFETs decreases with increasing gate voltage (to more positive voltage) as expected for p-type surface conductive layer. The transfer characteristics of NCD SGFETs were measured in amplification regime at Uds = −0.6 V [67]. Detailed information is in the attached publication "Function of thin film nanocrystalline diamond-protein SGFET independent of grain size".
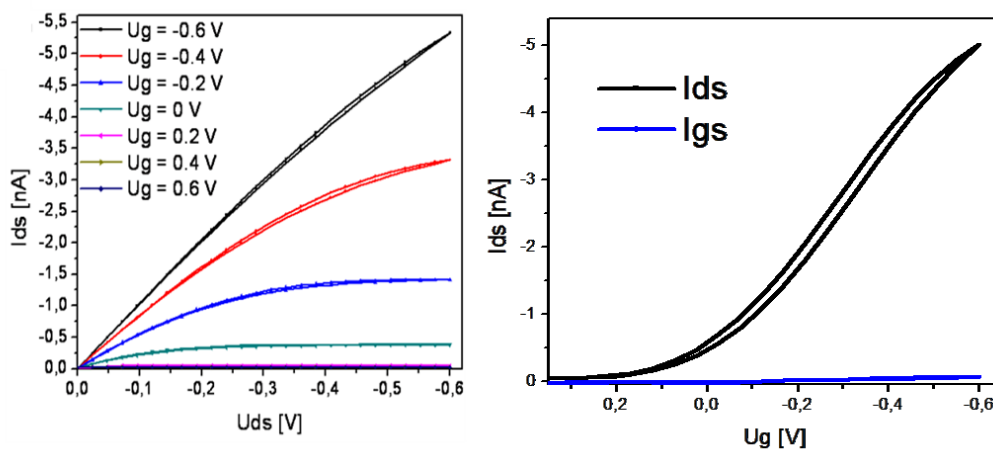
Figure 3.1: *Output characteristics (left), transfer and gate current characteristics (right) of pristine FET device measured in HEPES solution ((pH = 7.14). Transfer characteristic was measured at Uds =−0.6 V.*

We also investigated very thin NCD films growth by linear antenna microwave plasma CVD (LAMWP-CVD) process from CO_2 containing gas mixtures. The average grain size is in the range of 50 and 80 nm as estimated from the SEM image (Fig. 3.2a). Thickness of NCD film determined from cross-sectional SEM image is about 56 nm.
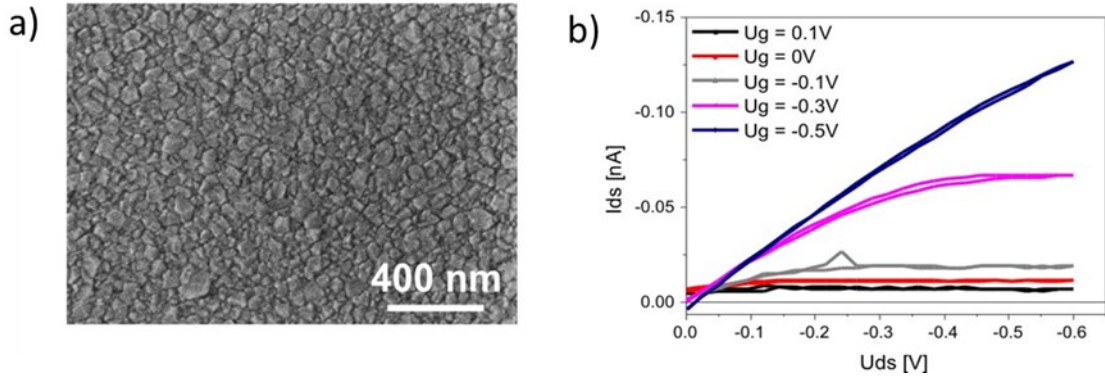
Figure 3.2: *SEM image of nanocrystalline diamond film grown by LAMWP-CVD on glass substrate (a) and output characteristics of nanocrystalline diamond solution-gated field-effect transistor measured in HEPES buffer solution at gate potentials from -0.5 to 0.1 V (b)* [84].

The output characteristics of nanocrystalline diamond SGFET measured in HEPES buffer solution at gate potentials from -0.5 to 0.1 V are presented in fig. 3.2b. Current-voltage characteristics show typical increase and saturation of the channel current Ids as a function of drain-source voltage Uds as well as modulation by gate voltage Ug. The channel current Ids decreases with increasing gate voltage (to more positive voltage) as expected for p-type surface conductive layer. Thus, these results prove transistor character of the SGFET based on NCD films grown by LAMWP-CVD. The transistor functionality is the same as in case of SGFET based on NCD films grown by focused plasma process [14,84]. We showed that even very thin NCD films growth by LAMWP-CV) process from CO_2 containing gas mixtures seem to be promising for fabrication of solution-gated field-effect transistors [84].

Before experiments with proteins and cells we solved several technical issues such as encapsulation of SGFET, electrical and mechanical stability, cracking of covering resists, toxicity and biocompatibility and optimizing of measurement setup

(Fig. 3.3). We tested different types of covering resins (ma15, ma40, SU8) with different thicknesses and different conditions of preparing to get optimal conditions for seeding of cells. The next chapter deals with stability of diamond SGFETs.
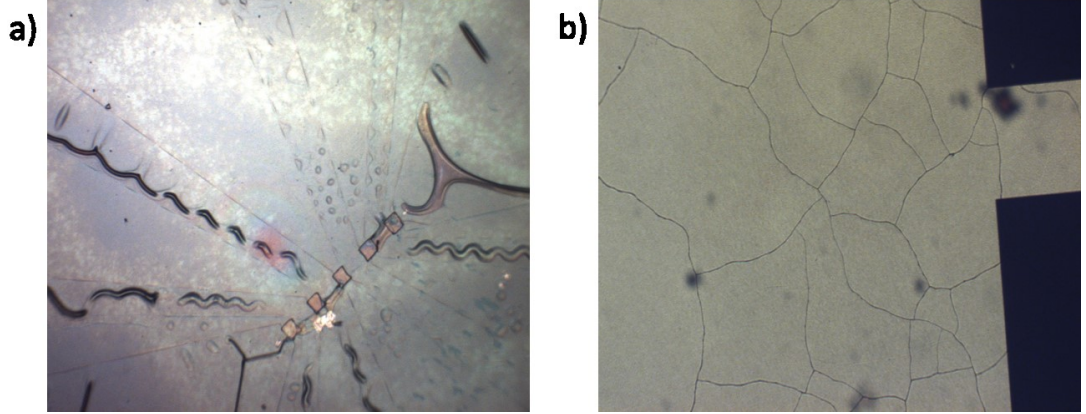
Figure 3.3: *Examples of technical problems: incorrect developing of negative covering resist SU8 (a) and cracking of positive covering resist ma40 (b).*

3.2 Stability of diamond SGFETs characteristics

Before experiments, the long-term and short-term stability of blank transistors measured in HEPES buffer was investigated.

Long-term stability of diamond SGFETs is different in various SGFET samples. We observed good stability of SGFETs for 8 days (see Fig. 3.4a). On the other hand, some SGFETs reveal negative gate voltage shift of transfer characteristics as well as decrease of Ids in long-term period (Fig. 3.4b). Figures 3.4c,d show percentage Ids decrease in dependence of time and percentage Ug shift in dependence of time for both stable and unstable FETs.

The reason of variable long-term stability is not clear. Measurements by Kelvin probe force microscopy (KPFM) showed that variability could relate to long-term change of H-terminated diamond itself. Possibly it could relate to surface oxidation, nitrogen impurities or degradation of H-termination as suggested by Geisler and Hugel [85]. Encapsulation of SGFETs also could play some role in long-

term stability. Other experiments can contribute to better understanding of these effects.
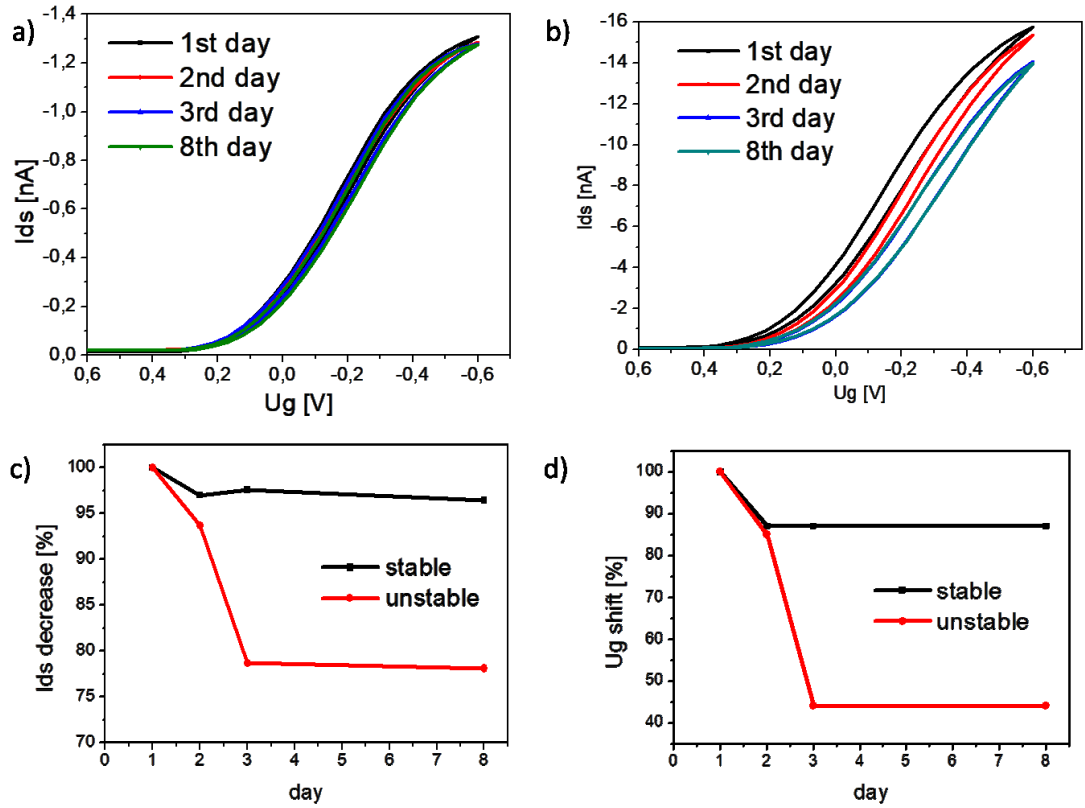
Figure 3.4: *Transfer characteristics of FET device measured in HEPES solution ((pH = 7.14) for stable SGFET with grain size of 80 nm (a) and unstable SGFET with grain size of 250 nm (b) measured for 8 days at the same conditions. Transfer characteristic was measured at Uds =−0.6 V. Percentage Ids decrease in dependence of time for stable and unstable SGFETS at Ug = -0.4V (c) and percentage Ug shift in dependence of time at Ids = -1 nA (stable SGFET) and Ids=-10 nA (unstable SGFET) (d).*

The transistor output, transfer, and gate leakage characteristics were measured using Keithley K327 source-measure units and custom made software package. The sweeping rate was 50 mV/s and the initial delay time was 5 s. Each characteristic was measured three times to obtain stabilized data. The third characteristic is stabilized in short term which is sufficient for our experiments (Fig. 3.5) [14,43,67].
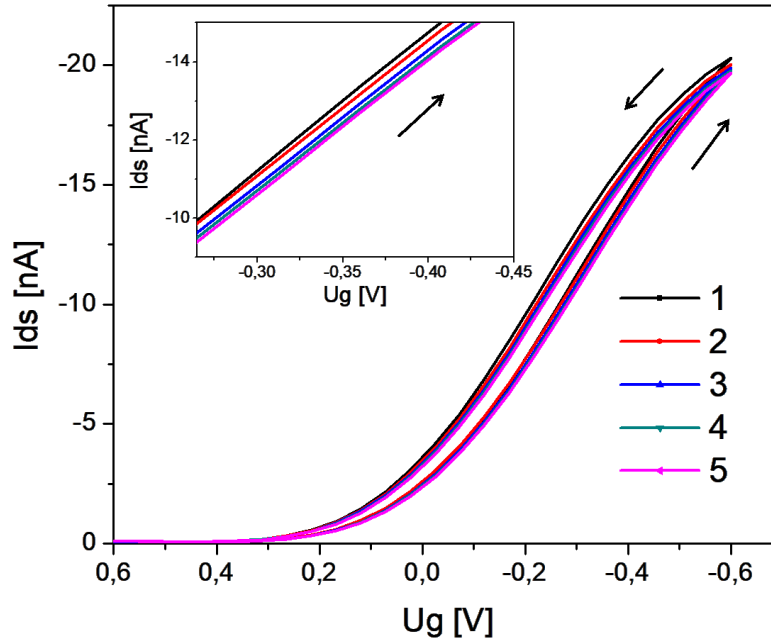
Figure 3.5: *Transfer characteristics of pristine FET device measured in HEPES solution ((pH = 7.14) for 5 times. Transfer characteristic was measured at Uds =−0.6 V. Inserted picture shows segment of transfer characteristics for Ug between -0.2 V and -0.4 V.*

3.3 Effects of protein layer on NCD SGFET characteristics

Fetal bovine serum (FBS) is a significant component of the cell medium and it contains crucial components for the cell growth; therefore we study its behavior on diamond [19].

Solution-gated FETs based on H-terminated nanocrystalline diamond films were employed for studying effects of fetal bovine serum (FBS) proteins on diamond electronic properties. FBS proteins adsorbed on the diamond FETs permanently decrease diamond conductivity as reflected by the −50mV shift of the FET transfer characteristics and the slope (transconductance) decreased. We found that this shift is permanent even after rinsing using deionized water, phosphate buffered saline and other agents and it is independent of grain size (Fig 3.6) [14,67].

Figure 3.6: *Transfer characteristics at Uds = −0.6 V of pristine device (black), after adsorption of FBS (red), after rinsing by deionized water (green) for NCD SGFETs with grain size of 250 nm.*

The shift is negative and leads to decrease of channel current, hence it cannot be explained as purely field effect where negative charge of proteins in FBS near physiological pH 7.4 should increase the channel current.

It is attributed to adsorption of a 2–4 nm primary protein layer from FBS which remains on diamond irrespective of rinsing as evidence by AFM [3,32] and which modifies original equilibrium of the surface conductive layer system by replacing ions in the very vicinity of the diamond surface like in the case of DNA molecules or lipid bilayers [86,87].

Fig. 3.7 shows the gate leakage currents of diamond SGFET in the initial pristine state (black curve) and after FBS adsorption (red curve) and after rinsing of FBS (blue curve) measured in pH 7 buffer as a function of gate voltage at fixed drain-source voltage of Uds =−0.6 V. The characteristics were measured by increasing gate potential from 0 V to −0.6 V. Most of the results indicated decrease in gate current after FBS adsorption. This can be explained simply by larger barrier for charge transfer across the diamond–electrolyte interface due to the additionally adsorbed layer. Yet some of the results showed increase in gate current after FBS adsorption which can mean that proteins can decrease the diamond–electrolyte electronic barrier induced by C−H surface dipoles and facilitate another route for

charge transfer across the interface [14] such as in the case of cytochrome proteins [88]. Schematic model is in chapter 3.5 (figure 3.14). For more details see the attached article "Effects of protein inter-layers on cell-diamond FET characteristics".
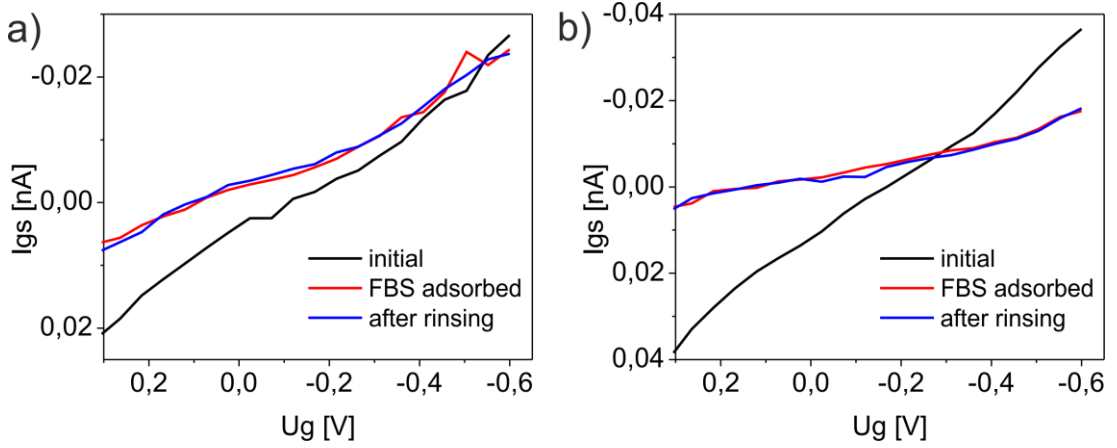
Figure 3.7: *Gate leakage currents of pristine diamond SGFET (black), after adsorption of fetal bovine serum (red), and after device rinsing (blue) as measured in pH 7 buffer at drain-source voltage Uds = −0.6 V for SGFET with grain size 250 nm (a) and 80 nm (b).*

3.4 Effects of cell growth on NCD SGFET characteristics

For diamond-based biosensors, understanding interaction between cells, proteins and solid-state surfaces is essential. The effect and contribution of proteins and cells to the electronic response of diamond SGFETs and to the electronic properties of diamond in general is vital for understanding the electronic response of such biosensors, yet it is still largely unexplored.

We present and discuss the influence of adsorbed FBS proteins and osteoblastic SAOS-2 cells on electronic properties of SGFETs based on H-terminated nanocrystalline diamond films exhibiting the surface conductivity. At first, effect of UV sterilization, an important step prior to the cell culture process, does not cause a further shift of transfer characteristics of NCD after FBS adsorption (fig. 3.8.) [67].
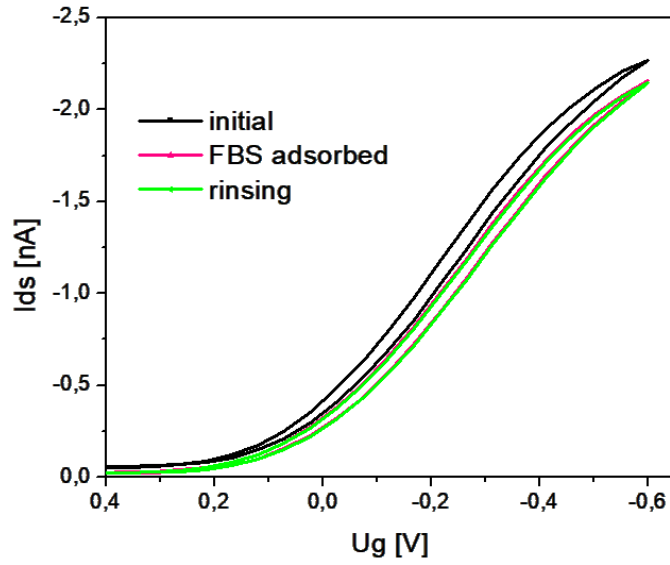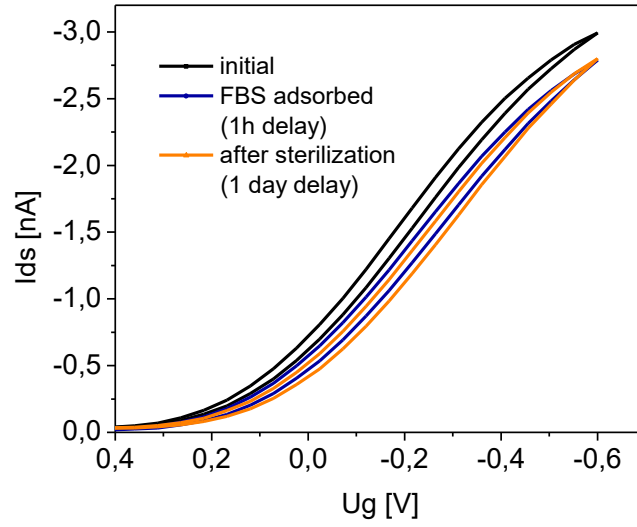
Figure 3.8: *Transfer characteristics at Uds = −0.6 V of pristine device (black), after adsorption of FBS (red), after sterilization (orange) for large grains measured in HEPES buffer.*

Fig. 3.9 shows the transfer characteristics and leakage currents measured at different stages. As reference initial stage, SGFET with absorbed FBS protein was used (Fig. 3.9a and b). As we showed in previous chapter the SGFET transfer characteristics after FBS adsorption is shifted by −50 mV, which is permanent even after rinsing using deionized water and phosphate buffered saline [14,67]. Additional shift of transfer characteristics was observed after the cell growth and delamination (−115 ± 10 mV at Ids= −2 nA) (Fig. 3.9f and g).
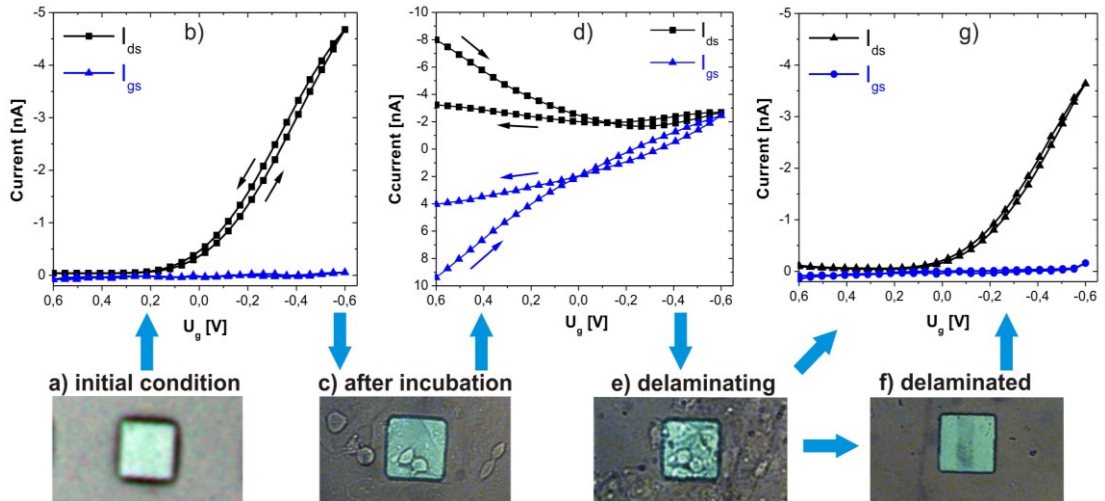
Figure 3.9: *Transfer characteristics and leakage currents at Uds= −0.6 V of NCD SGFETs with large grain size measured: (b) after FBS protein absorption (labeled as "initial"), (d)after cell incubation and (g) during or after full delamination of cells. Fig. (a), (c), (e), (f) are optical photos of transistor openings at the specific stage of the measurement (rectangular squares represent the transistor opening areas with size of 60 m × 60 m).*

However, just after the cell growth (i.e. cell incubation), the transistors reproducibly exhibited increased leakage currents (Igs) up to 10 nA at the gate voltage of 0.6 V (Fig. 3.9d). We observed that after the cell incubation and before measurements the cells are spread well on the active gate area (Fig. 3.9c), but due to measurement of SGFET transfer characteristics the cells are delaminating from the diamond surface, which is shown by changed contrast in the cell optical images (Fig. 3.9e).

After the cell delamination and/or full removal, the transistors returned to full functionality (except for a persistent −115 mV shift of the transfer characteristics) with leakage currents close to ±0.15 nA (Fig. 3.9g). This effect is reproducible. It was observed also for repeated cell incubation on the same sample, and for all our NCD SGFETs used for repeated measurements (Fig. 3.10).
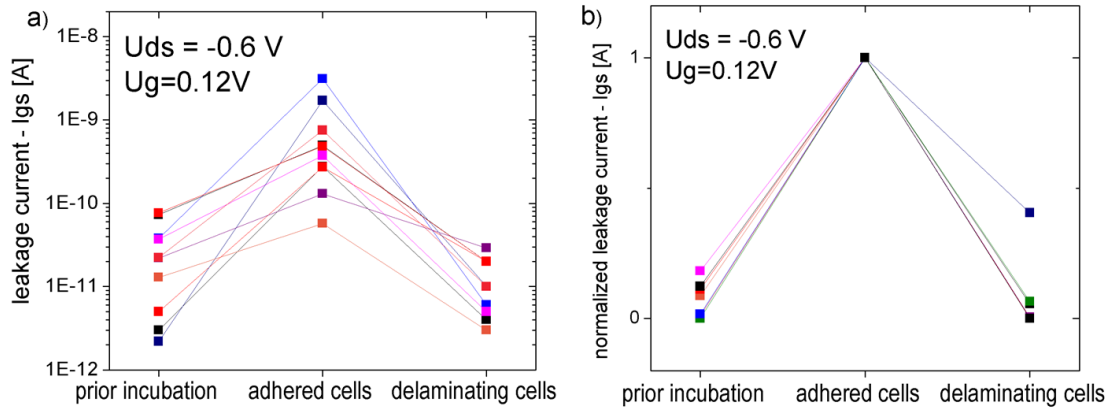
Figure 3.10: *Raw (a) and normalized (b) leakage currents of several NCD SGFETs measured at different stages of the cell delamination effect. The leakage currents are plotted at Ug= 0.12 V and Uds= −0.6 V .*

Fig. 3.11 shows the schematic model of cell delamination due to leakage currents. At first, the H-terminated surface of the active gate area is fully covered by FBS proteins, which change the surface properties [14] and create the initial condition for our experiments (Fig. 3.11a). After the cell incubation (i.e. before measurement of the SGFET transfer characteristics with cells), the cells are spread well across the gate area and adhered to the protein layer (Fig. 3.11b). After starting the measurements, a leakage current flows between the source and gate electrode and it initiates delamination of the cells from the diamond surface (Fig. 3.11c). In this

stage as well as after complete removal of the cells, the transistor gate currents recover to original values.
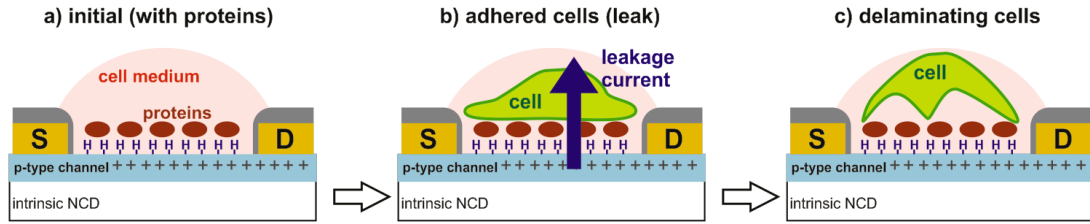
Figure 3.11: *Schematic model of cell–protein–diamond interface on H-terminated diamond SGFET under different conditions: (a) initial stage with adsorbed FBS proteins on the gate area, (b) well adhered cells after incubation and at the beginning of the measurements, (c) delaminating cells and persistent protein layer.*

We proposed a mechanism of this trigger effect. We attribute it to a close interaction between diamond and cell membrane that releases excess ions to the interface. This interaction becomes negligible when the cells change shape and delaminate. Study of non-adherent yeast cells showed that leakage current did not increase during cell cultivation unlike in our case of adherent cells which confirms our suggested mechanism [36]. For more details see the attached article "Osteoblastic cells trigger gate currents on nanocrystalline diamond transistor". This effect could be thus used as a mechanism for electrical sensing of cell adhesion and cell culture quality, e.g. for in vivo like perfusion systems [89].

3.5 Role of grain boundaries in diamond SGFETs

From electronic point of view NCD is a complicated system due to the presence of sp2 carbon phase and grain boundaries and role of these features for biosensors and bioelectronics is not yet understood. Therefore, we employed NCD films of different grain sizes of 250 and 80 nm (figure 3.12a and 3.12b) to characterize and discuss influence of grain boundaries and sp2 phase on protein adsorption and electronic function of solution-gated field-effect transistors.

The thicknesses of the diamond films as calculated from the AFM are 445±27 nm and 108±19 nm depending on the grain size (error bars are given by root-mean-

square roughness of the films as obtained by AFM in the area of 5µm × 5 µm). We have shown that intrinsic nanocrystalline diamond films with average grain sizes down to 80 nm, thickness down to 100 nm, and p-type surface conductivity generated by H-terminated surface are fully operational as SGFETs on glass substrates. Fig. 3.12c and 3.12d show the output characteristics measured at gate voltages from 0.6 V to −0.6 V. They prove transistor character of the NCD SGFETs [67].
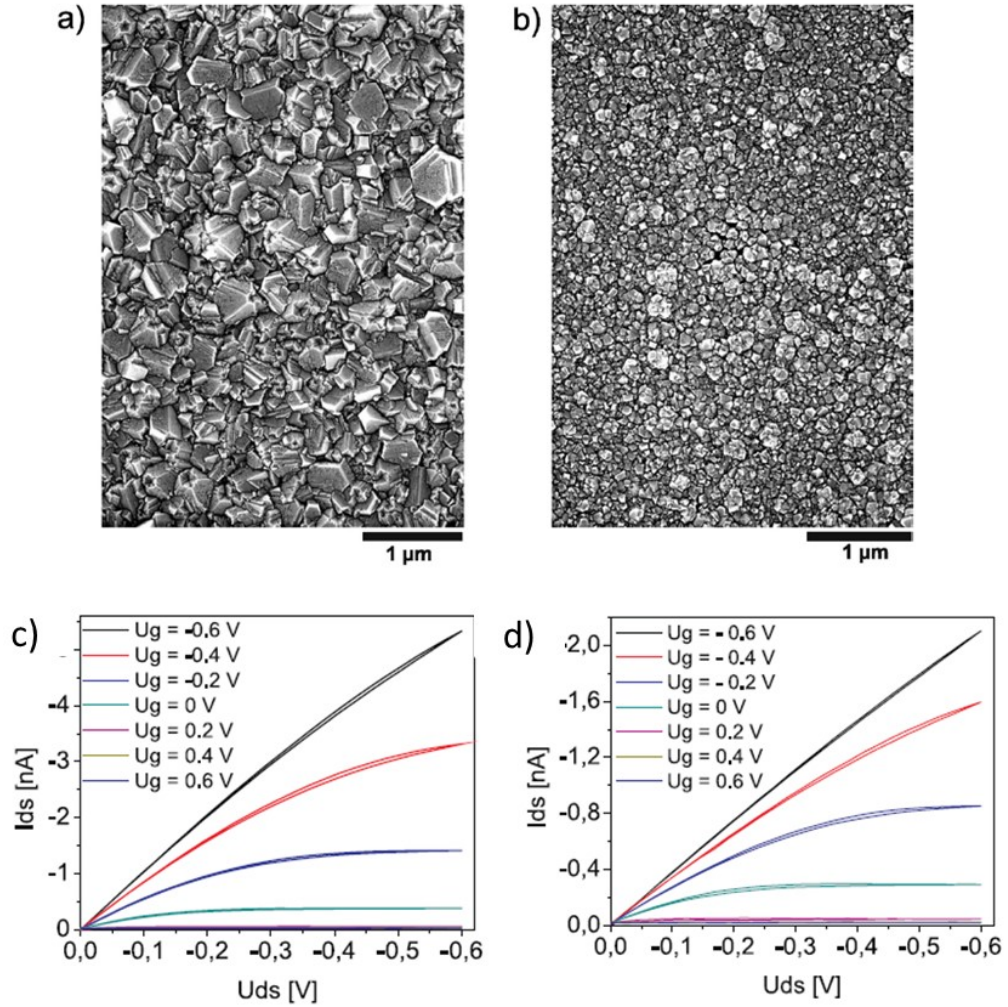
Figure 3.12: *SEM images of nanodiamond surfaces with average grain size of 250 nm (a) and 80 nm (b). Output characteristics measured in HEPES solution, grain size of NCD 250 nm (a) and 80 nm (b).*

The transfer characteristics of NCD SGFETs were measured in amplification regime at U_{ds} = −0.6 V. The transconductance of the SGFETs, defined as g_m = $\delta I_{ds}/\delta U_g$ and calculated at I_{ds} in the linear region of transfer characteristics is 8.9 nS at U_{ds} = −0.6 V, I_{ds} = −2.5 nA for SGFET with grain size 250 nm and it is 3.0 nS at

Uds = −0.6 V, Ids = −1.0 nA for SGFET with grain size 80 nm. Using these parameters, gains (defined as g_m × Uds/Ids) of the SGFETs are 2.2 and 1.8 for SGFET with grain size 250 nm and 80 nm, respectively. SGFET with smaller grains has overall smaller conductivity because of high number of grain boundaries which limit the electronic transport [65] and smaller transconductance yet its gain is comparable to SGFET with larger diamond grains.

The SGFET conductivity decreased after application of FBS as reflected by the shift of SGFET transfer characteristics by −50 mV and by the decreased slope (transconductance) (Fig. 3.13). We found that this shift is permanent even after rinsing using deionized water and phosphate buffered saline, in full agreement with our other experiments (more details are in attached paper "Effects of protein inter-layers on cell-diamond FET characteristics") and it is independent of grain size. In our case we observe that this effect is independent of the grain size and thus independent of grain boundaries and overall sp2 content. This was observed systematically on various sets of samples. Obviously, even on nanocrystalline diamond it is the surface of diamond grains that controls the diamond–protein interaction.
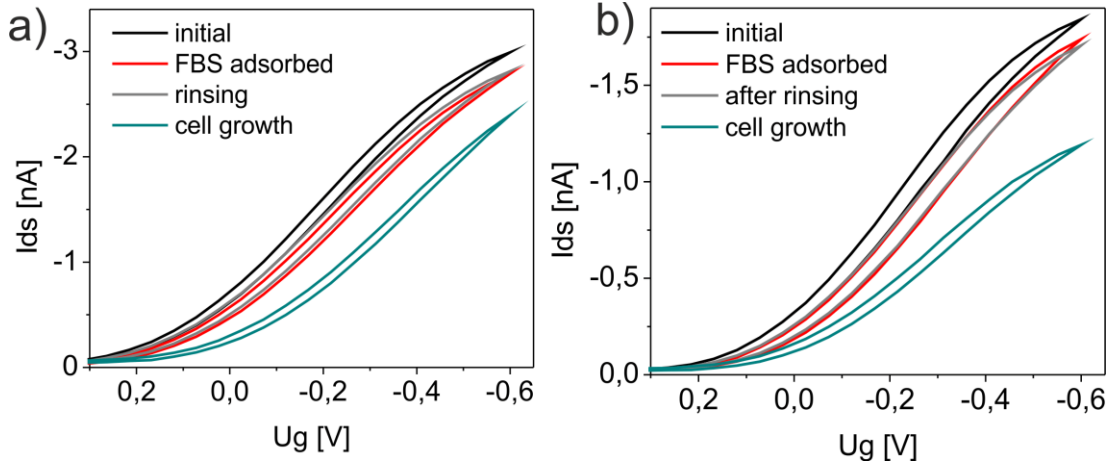
Figure 3.13: *Transfer characteristics at Uds = −0.6 V of pristine device (black), after adsorption of FBS (red), after rinsing by deionized water (blue), and after cell culturing process (green) for NCD SGFETs with grain size of 250 nm (a) and 80 nm (b).*

The protein layer also changed gate (leakage) currents as shown in Fig. 3.7 for NCD SGFETs with different grain size (250 nm and 80 nm). The range of gate

currents 10–40 pA is comparable on both devices in spite of significant difference in grain size, density of grain boundaries and sp2 phase. Considering that the effects are similar for both SGFETs with different grain size and different density of grain boundaries we suggest that the gate currents are determined by the barrier of H-terminated surface itself [24] as well as by its additional interaction with adsorbed protein layer.

We found that inherent hysteresis of SGFET transfer characteristics, their reaction time, their negative shift after protein adsorption and cell culturing process, low gate leakage currents and no influence of UV sterilization or rinsing are all independent of the NCD grain size. Thus we proposed a microscopic model where the function of NCD SGFET is determined by the H-terminated surface of diamond nanocrystals and its interaction with proteins, not by grain boundaries or sp2 phase in general (Fig 3.14). Detailed information is in the attached publication "Function of thin film nanocrystalline diamond-protein SGFET independent of grain size".
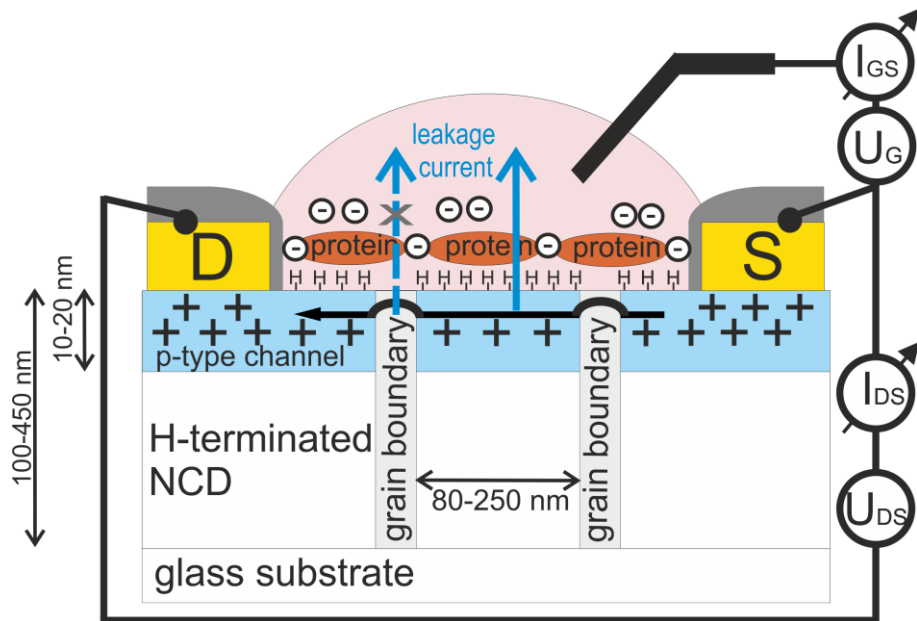
Figure 3.14: *Schematic model of the interface between H-terminated nanocrystalline diamond and cell medium containing proteins from fetal bovine serum.*

3.6 Renewal of directly grown diamond SGFETs by hydrogenation

As mentioned in previous chapters FBS protein layer is persistent on diamond surface even after rinsing with inorganic solutions (NaOH), detergents (sodium dodecyl sulfate), phosphate buffered saline, enzymes etc.

We studied possibilities of renewal of the directly grown three-dimensional diamond transistors including the encapsulation and gold contacts by low temperature hydrogenation which should not damage resists and demarcation of channels.

We compared both organic resins (MA-P, OFPR, and SU8) and silicon nitride (Si_3N_4) as encapsulation materials. We studied if such complete encapsulated devices can be recycled after low temperature hydrogenation (LTH) [81] process via cleaning the gate surface from proteins and at the same time preserving H-termination of diamond surface. We characterized effects of low temperature hydrogen plasma treatment (200–300 °C) in two different microwave plasma reactors (linear and focused plasma) on diamond transistor characteristics and on etching of organic resin and silicon nitride encapsulation.

2 μm   Z scale=10nm   2 μm   Z scale=10nm   2 μm   Z scale=10nm
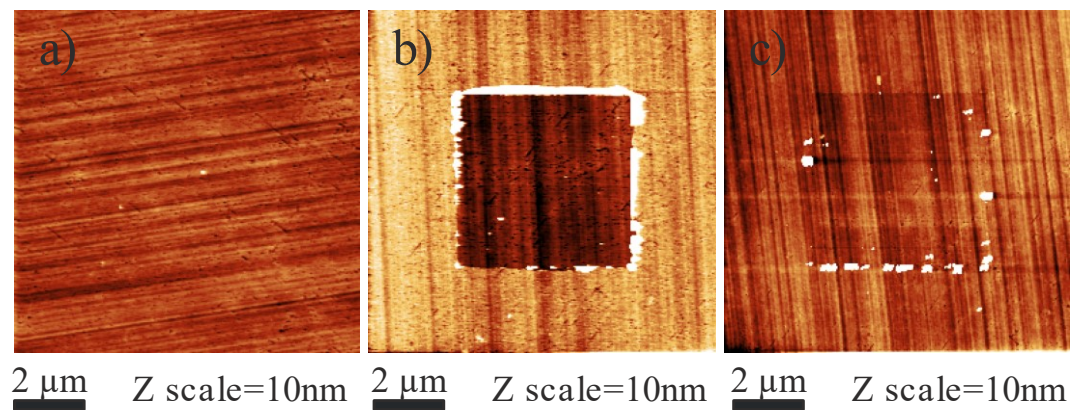
Figure 3.15: *AFM characterization of diamond surface (a) and protein layer before (b) and after low-T hydrogenation (c).*

After the FET characteristic measurements the samples were recycled by the LTH. Fig. 3.15 shows AFM images of diamond surface and protein layer before and after low-temperature hydrogenation. By using the AFM nanoshaving method, Fig.

3.15b evidences the presence of such protein layer also here, compared to the initial surface. Moreover, Fig. 3.15c shows that the low temperature hydrogen termination in linear antenna plasma (at 200 °C) successfully removed this FBS protein layer from the monocrystalline diamond surface (unlike rinsing in the solutions). Only < 1 nm thin layer (probably some residual hydrocarbons from the plasma process) remains on the surface which should be taken into account in further experiments.

The Fig. 3.16 evidences that the directly grown FETs are still fully operational after LTH at 200 °C in linear plasma reactor even after repeated LTH process.
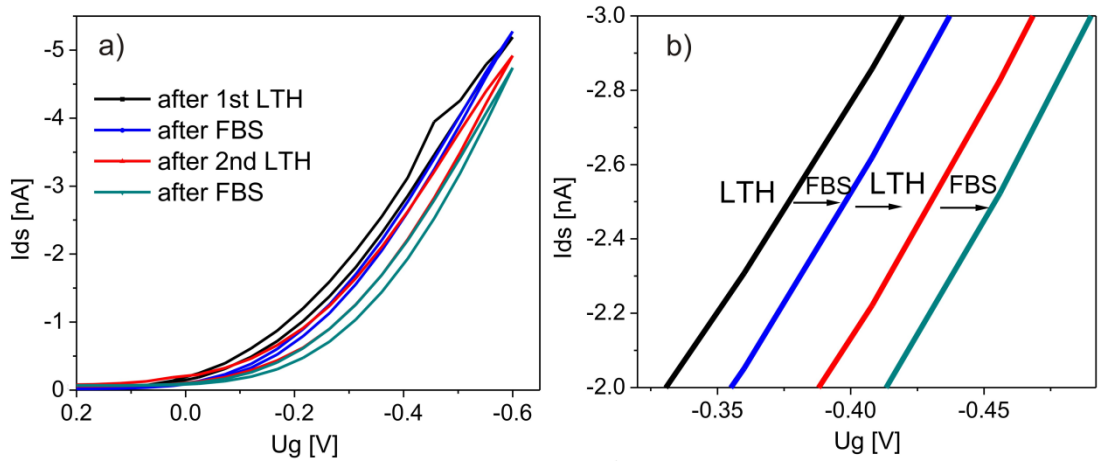
Figure 3.16: *Transistor characteristics after repeated LTH process in linear plasma at 200 °C and after FBS adsorption (a) and magnified part of the transfer characteristics showing FET response for one Ug sweep direction (b). All transfer characteristics were measured in HEPES at Uds = -0.6 V.*

Applying FBS proteins on diamond solution-gated FET after repeated LTH process at 200 °C caused the same shift of transfer characteristic (-30 mV) like in the case of FBS adsorption on initial diamond FET (Fig. 3.16b). Thus, sensitivity of encapsulated diamond-protein transistor is renewed by low temperature hydrogen plasma.

Fig. 3.17 shows etching rates after LTH for different types of encapsulation and temperatures. All the data are related to linear plasma except for SU8 3010 and for Si_3N_4 ("stars") which have been obtained after LTH in the focused plasma at 300 °C. If the resins where fully removed after the LTH process, the etching rates were determined as bottom estimates based on the initial resin thickness.
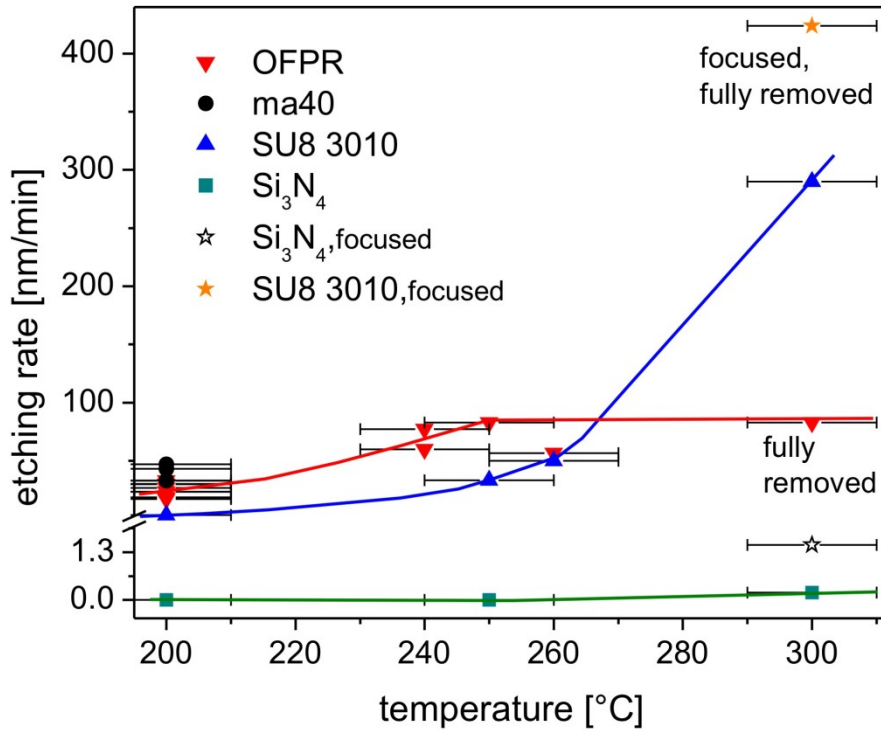
Figure 3.17: *Etching rates for photoresists (OFPR, ma40 and SU8 3010) and for silicon nitride as a function of temperature.*

LTH in the linear plasma is less aggressive to encapsulation than focused plasma most likely due to larger distance (7 cm) between the high density plasma region and the sample surface [64,81]. In the focused plasma the sample is in or in the very vicinity of plasma ball. We observed increased etching rates (from 3 to 400 nm/min for photoresists and from 0 to 1.5 nm/min for Si_3N_4) as a function of hydrogenation temperature (200–300 °C). Based on the data of LTH in the linear plasma, photoresist SU8 is the most stable of the employed organic resins and it can be used up to 300 °C.

As for gold contacts, their quality appears good even after LTH in the focused plasma.

We show that low temperature hydrogenation at linear plasma system is more suitable due to larger distance between the high-density plasma region and the sample surface. It is less aggressive on encapsulation and 3D transistors are fully operational after this treatment.

The directly grown three-dimensional diamond transistors including the encapsulation and gold contacts can be recycled by low temperature hydrogenation in linear antenna reactor within 30 minutes without any further processing. Detailed

information is in the attached publication "Sensitivity of encapsulated diamond-protein transistor renewed by low temperature hydrogen plasma".

3.7 Radiation experiments

Diamond is considered as a promising tissue equivalent material in radiation therapies as well as for bio-electronic sensors therefore effects of gamma irradiation on function and stability of hydrogen-terminated diamond SGFETs were studied. Our experiments include irradiation of blank diamond SGFETs, SGFETs with proteins and SGFETs with cells.

Irradiation of diamond SGFETs (without proteins/cells)

Transfer characteristics of the diamond SGFET before and after the gamma irradiation by 5 Gy are shown in Fig. 3.18. The measurement was done in HEPES buffer without proteins and without cells. Both transfer curves reveal a small hysteresis (up to 20mV) and only a small negative voltage shift around −10 mV is observed for the gamma irradiated diamond SGFET (blue curve in Fig. 3.18a). This voltage shift is actually smaller than the observed shift after the protein adsorption (about −50 mV) [14]. Unlike typical protein adsorption experiments performed within 1 h, our measurements also confirm the long-term stability while delay times between both measurements were from1 to 3 days. Therefore, we proposed that the observed shift in transfer characteristics is most likely attributed to the transistor drift. For the gate currents we observed almost the same curves measured before and after the transistor irradiation (Fig. 3.18b). The transfer and gate current characteristics of the employed diamond SGFET indicate its radiation resistance to doses as high as 5 Gy.
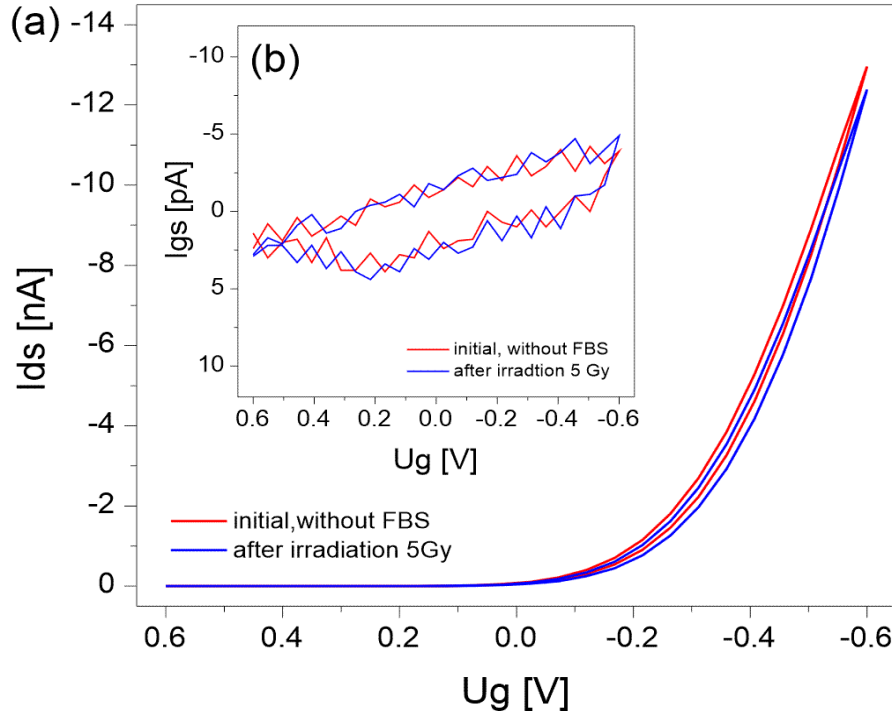
Figure 3.18: *Transfer (a) and gate current (b) characteristics of diamond SGFET at Uds=−0.6 V measured before and after the irradiation by 5 Gy. Electrical measurements were done in HEPES buffer without FBS and without cells.*

Irradiation of diamond SGFETs with proteins (without cells)

Next, we investigated the functionality of γ-irradiated diamond SGFET with proteins adsorbed from the fetal bovine serum. The results for 2 Gy and 5 Gy irradiations are shown in Fig. 3.19. The transfer characteristic of diamond transistor with HEPES and proteins exhibited a negative voltage shift by –31 mV in comparison to the bare diamond transistor (red vs. black curve, Fig. 3.19a). The gate current decreased from 11 pA to 6 pA after applying FBS (black vs. red curve, Fig. 3.19b). After irradiation by 2 Gy the transfer characteristic of SGFET with FBS exhibited a positive gate voltage shift by +20mV. At the same time the gate current increased from 6 pA to 15 pA (red vs. blue curve, Fig. 3.19b). In another case, after irradiation by 5 Gy, the transfer characteristic of SGFET with FBS exhibited a more commonly observed negative gate voltage shift by −150 mV (red vs. black curve, Fig. 3.19c).
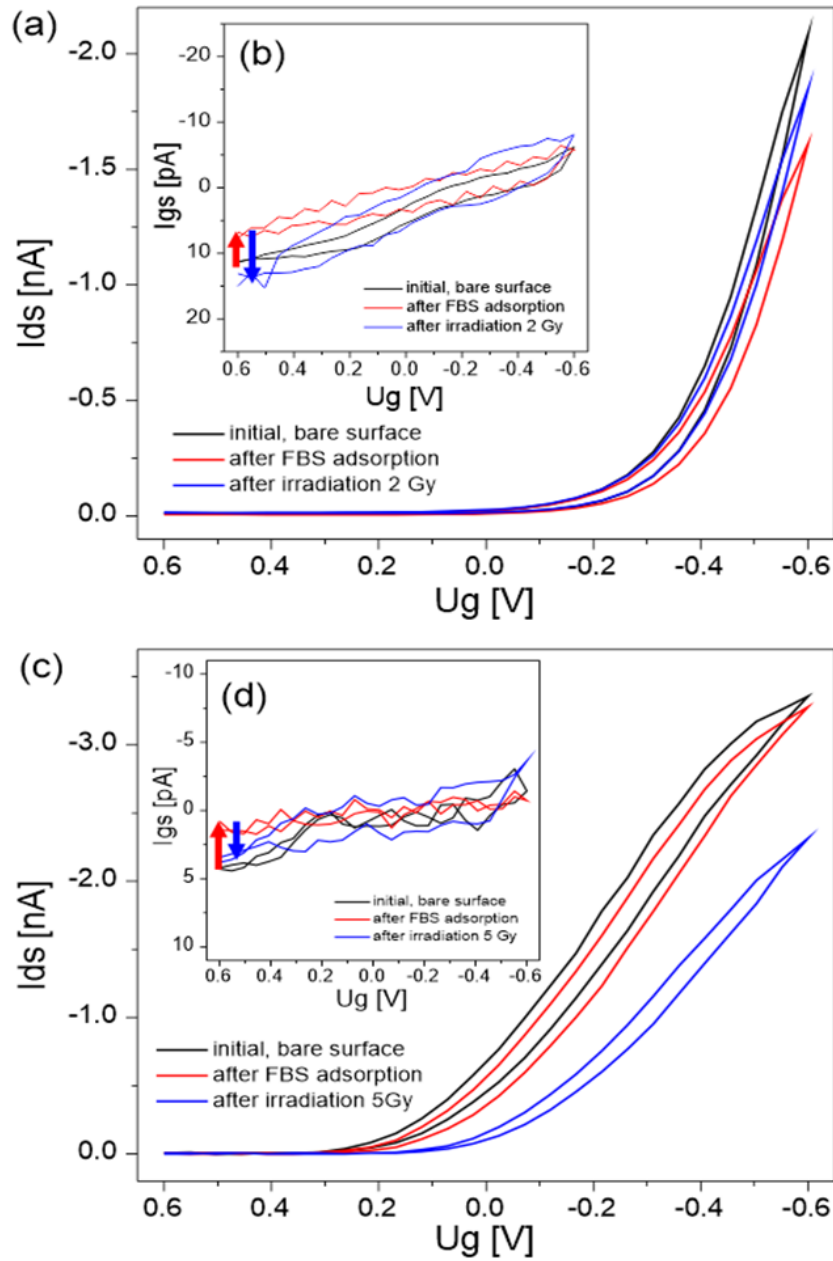
Figure 3.19: *Transfer (a,c) and gate current (b,d) characteristics of two different diamond SGFETs at Uds = −0.6 V. The SG-FETs were measured in HEPES medium with FBS without cells before and after the irradiation by (a,b) 2 Gy and (c,d) 5 Gy.*

Irradiation of diamond SGFETs with proteins and cells

Fig. 3.20 a–c show optical images of the active channel area (the central square) of diamond SGFETs with cultivated SAOS-2 cells before and after the gamma irradiation. Before the irradiation, cells well spread even on H-terminated diamond channel due to high enough density of cells and mutual cell communication [19]. As a simplified graphical view, the initial transfer characteristic is plotted for the diamond SGFET measured with HEPES medium and FBS (black curve, Fig.

3.20d) before the irradiation. The gate current characteristic reveals a narrow hysteresis and relatively low gate currents (11 pA at Ug = 0.6 V). After the cell growth, we observed an additional negative voltage shift. The voltage shift between the blank (no FBS & no cells) and the SGFET with cells was as high as −100 mV.

The optical image of the diamond SGFET irradiated by 5 Gy (Fig. 3.20b) confirms the presence of surviving cells in the active area (Fig. 3.20a). The transfer characteristic (blue curve, Fig. 3.20d) keeps the negative shift in comparison to the initial SGFET characteristic measured in HEPES medium with FBS. Noticeable is corresponding increase of the gate current to 60 pA for Ug = 0.6 V.
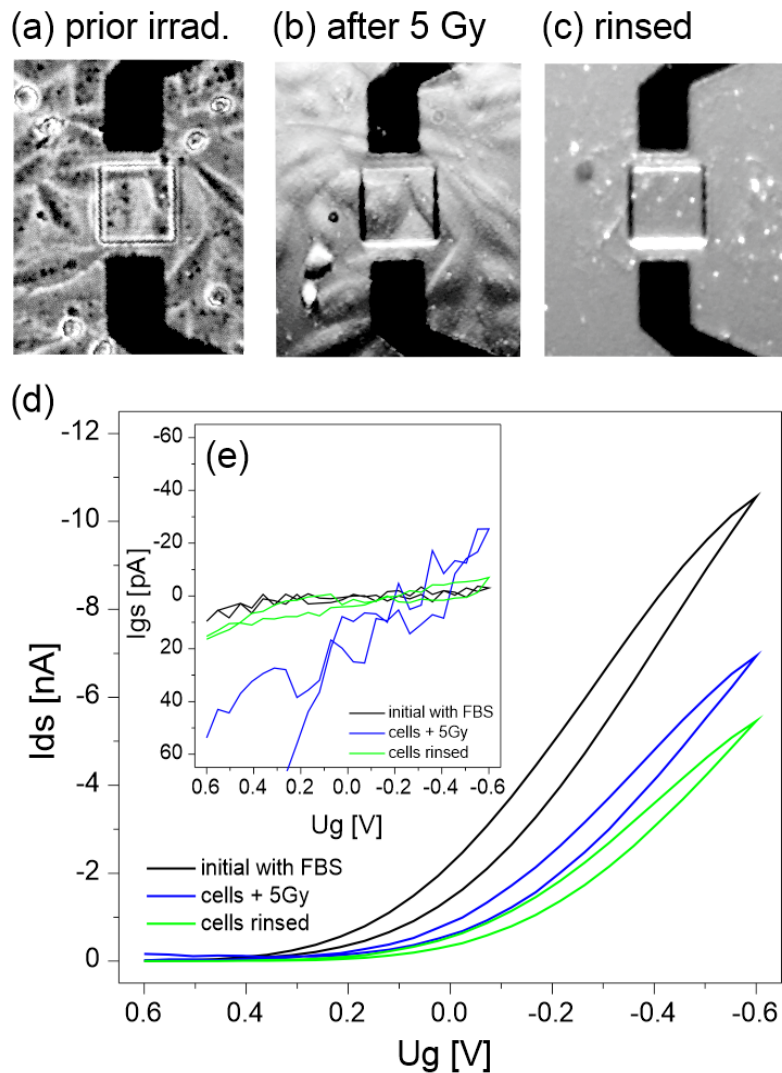
Figure 3.20: *Optical images of the active channel area (the central square) of diamond SGFETs with cultivated SAOS-2 cell before (a) and after (b) the gamma irradiation, and cell rinsed (c). Transfer (d) and gate current (e) characteristics of the SGFET at Uds = −0.6 V measured in HEPES medium with FBS,with cells irradiated by 5 Gy and after rinsing in deionized water.*

AFM measurements

In order to understand the increase in gate currents and transfer characteristic shifts we performed AFM characterization of FBS protein layers adsorbed on H-terminated monocrystalline diamond with atomically flat surface (for details see experimental part and Ref. [19]. Fig. 3.21 shows the surface morphology as a function of the irradiation dose (0 to 300 Gy). Prior to the gamma treatment (0 Gy) the adsorbed layer is about 5 nm thin, flat (RMS roughness 1 nm) and contains small bio-molecules (20–25 nm wide, 3–5 nm tall) [19]. The density and size of adsorbed features (white dots and areas) increased for dose as low as 5 Gy. The surface roughness increased from 1 to 2 nm. The same trend was observed also for higher irradiation doses. For the dose of 100 Gy, the roughness steeply rose to 6 nm and then saturated at around 8 nm for 300 Gy. The AFM characteristics suggest that the proteins or some other components from FBS agglomerate due to the gamma irradiation.

(a) 0 Gy   (b) 5 Gy   (c) 100 Gy   (d) 300 Gy

200 nm   Z scale=10 nm   200 nm   Z scale=10 nm   200 nm   Z scale=10 nm   200 nm   Z scale=10 nm

RMS=1.0 nm, Lx=88 nm   RMS=2.0 nm, Lx=63 nm   RMS=6.2 nm, Lx=59 nm   RMS=8.0 nm, Lx=109 nm
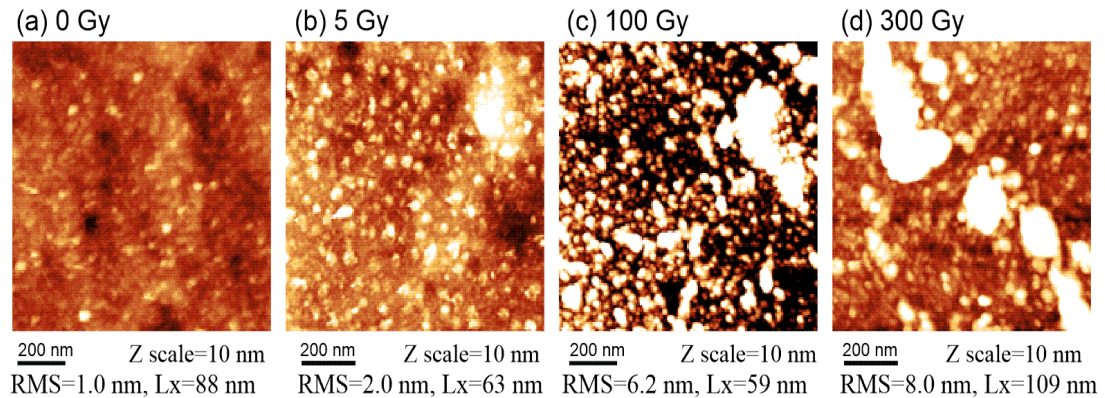
Figure 3.21: *Surface topography of monocrystalline diamond with adsorbed layer after the gamma irradiation at various doses from 0 to 300 Gy. The Lx corresponds to autocorrelation length, i.e. to the characteristic lateral dimension along the x-axis.*

The results of the above mentioned experiments showed that the nanocrystalline diamond SGFETs based on H-terminated surface conductivity are gamma radiation resistant. Moreover, we showed that changes in the SGFET transistor characteristics after the irradiation can be attributed to the radiation-induced modifications of bio-layer (proteins, cells, etc.) on the diamond surface. For

the blank SGFET the transfer and leakage current characteristics were stable after the gamma irradiation up to 5 Gy. The irradiated SGFETs with adhered proteins and cells were functional. Observed changes in gate current characteristics were assigned to modified morphology of proteins and cells on the H-diamond surface due to the γ-irradiation. After cell rinsing, a recovery of SGFET characteristics to initial-like curves was observed.

The presented results establish a first step towards real-time electronic monitoring of cell growth during the irradiation by therapeutically relevant doses. For more details see the attached publication "Gamma radiation effects on hydrogen-terminated nanocrystalline diamond bio-transistors".

3.8 Portable demonstrator

For applications in clinical environment, more compact, portable and uncomplicated device is needed. Thus we developed a demonstrator with in-plane gate electrode and placeable sensor chips (Fig. 3.22). Design of electronic circuitry and assembly of the demonstrator unit was done by Ing. Pavel Kulha from the Faculty of Electrical Engineering, CTU in Prague.
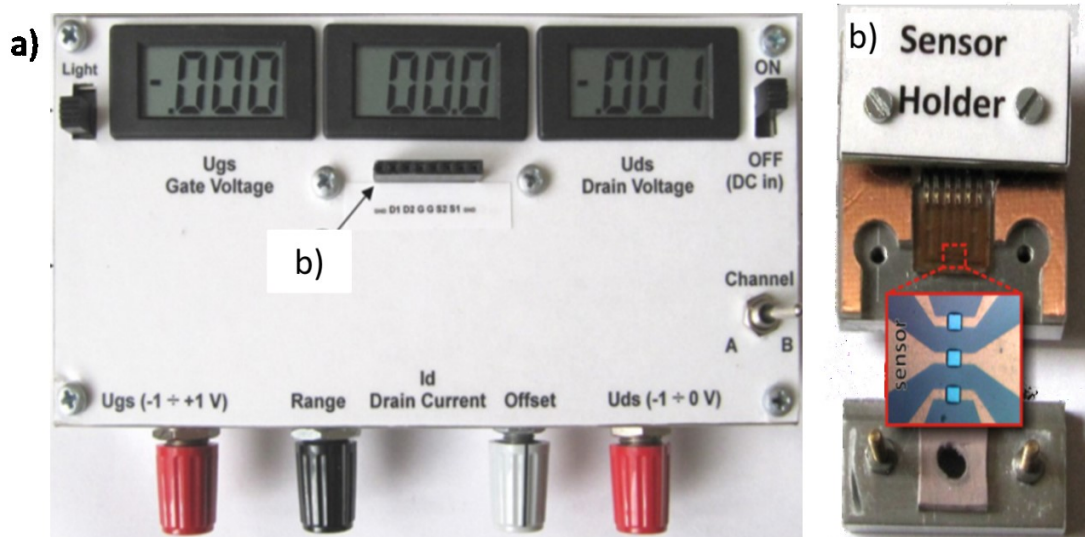
Figure 3.22: *Demonstrator with in-plane gate electrode (a) and placeable sensor chips (b).*

For these experiments we prepared in-plane NCD SGFETs with platinum gate and 2 channels (Fig. 3.23).
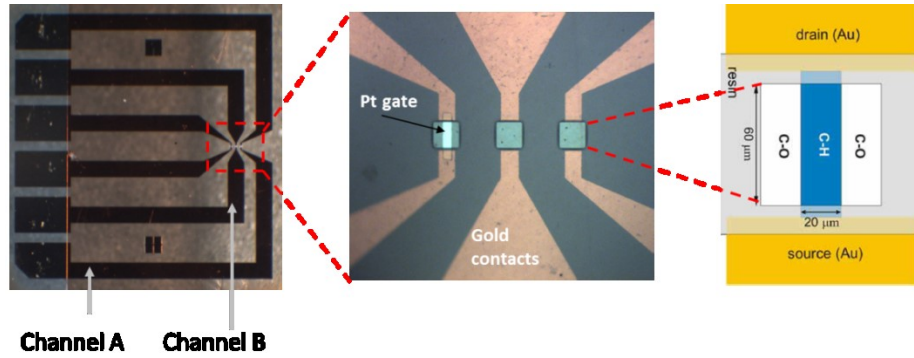
Figure 3.23: *In- plane gate FET based on NCD with Pt gate. Optical image of whole in-plane gate FET (left), section with Pt gate and 2 channels (middle) and opening of 60μm × 60 μm in covering insulating resin and active H-terminated diamond gate area of 20 μm × 60 μm (right).*
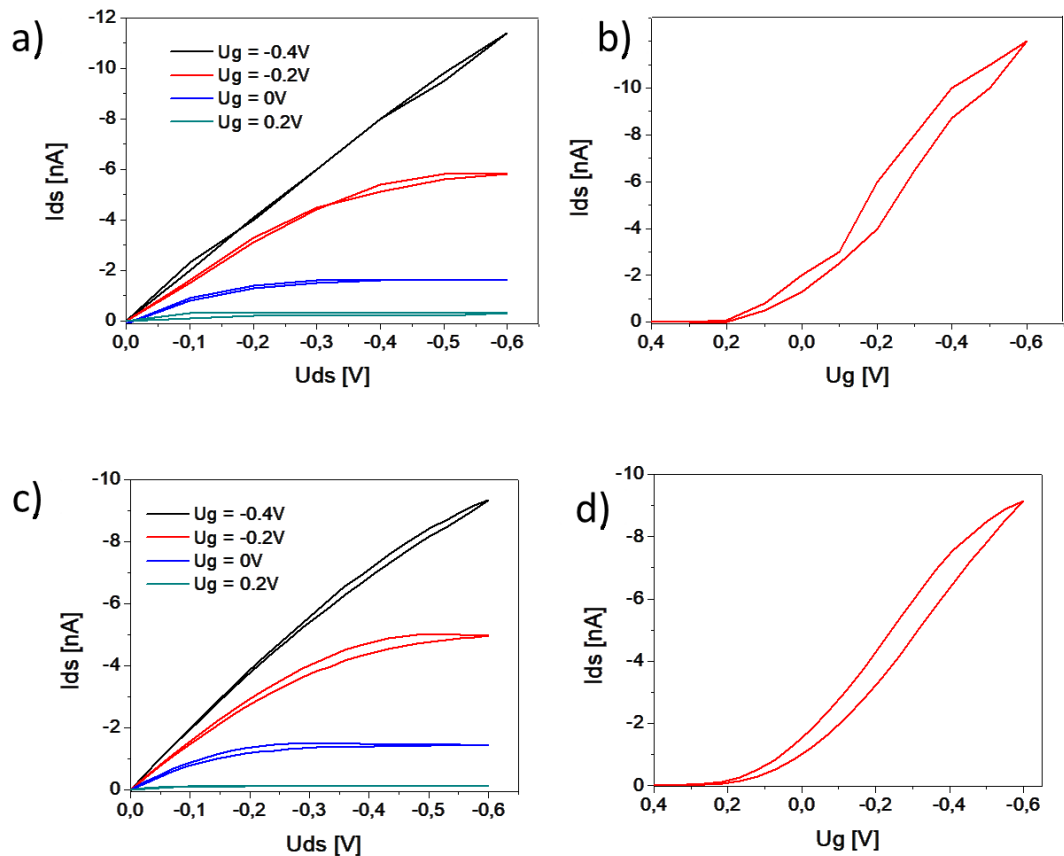
Figure 3.24: *Output characteristics (a) and transfer characteristics at Uds = −0.6 V (b) measured by demonstrator. Output characteristics (c) and transfer characteristics at Uds = −0.6 V (d) measured by Keithley devices. All characteristics were measured in HEPES.*

Output and transfer characteristics (measured at Uds = -0.6 V) measured by portable demonstrator are qualitative comparable (including hysteresis) with characteristics measured by the sophisticated setup with Keithley source-measure units, reference micro-electrode, positioners, Faraday cage etc. (Fig. 3.24). Only measured values of Ids are slightly higher for demonstrator. The reason is not clear yet but the difference is not significant. Thus portable demonstrator with in-plane gate electrode can be employed for measurement output and transfer characteristics of SGFETs.

4 Conclusions

This thesis presents the research conducted towards fabrication, characterization and employment of diamond SGFETs. We have shown that solution-gated field-effect transistors based on H-terminated nanocrystalline diamond films exhibiting surface conductivity and without gate oxides are fully operational in biologically relevant environments.

The most important conclusions of this thesis can be summarized in several points:

1. We optimized fabrication of diamond SGFETs and solved several technical problems concerning applying of different covering resists with different thickness, their instability, cracking and possible toxicity.

2. We showed that NCD with grain sizes down to 80 nm and film thickness of 100 nm prepared by focused plasma process as well as very thin NCD films growth by linear antenna microwave plasma CVD process are fully operational as SGFET and can serve as transducers (and partly also as amplifiers) of biological and/or environmental characteristics to electrical signals.

3. Adsorption of proteins from the cell growth medium (McCoy's 5A) containing 15% FBS lead to the shift of the SGFET transfer characteristics by −50 mV. This shift is permanent and it is due to the formation of 2–4 nm thin protein layer on the diamond as confirmed by AFM studies.

4. We found that inherent hysteresis of SGFET transfer characteristics, their reaction time, their negative shift after protein adsorption and cell culturing process, low gate leakage currents and no influence of UV sterilization or rinsing are all independent of the NCD grain size. We propose a microscopic model where the function of NCD SGFET is determined by the H-terminated surface of diamond nanocrystals and its interaction with proteins, not by grain boundaries or sp2 phase in general.

5. After cell cultivation, the transistors exhibit about 100× increased leakage currents (up to 10 nA). During and after the cell delamination, the transistors return to original gate currents. We proposed a mechanism where this

triggering effect is attributed to ions released from adhered cells, which depends on the cell adhesion morphology, and could be used for cell culture monitoring. It was later confirmed by study on non-adherent cells, where the transistor operated normally even with cells.

6. The directly grown three-dimensional diamond transistors including the encapsulation and gold contacts can be recycled by low temperature hydrogenation in linear antenna reactor within 30 minutes without any further processing.

7. We showed that the nanocrystalline diamond SGFETs based on H-terminated surface conductivity are gamma radiation resistant resistant and changes in the SGFET transistor characteristics after irradiation can be attributed to the radiation-induced modifications of bio-layer (proteins, cells, etc.) on the diamond surface. The presented results establish a first step towards real-time electronic monitoring of cell growth during the irradiation by therapeutically relevant doses.

8. Finally, we applied our findings and technical solutions to make battery-driven device that can be employed for class-room or field use.

The author's contribution

The author did all preparation steps concerning fabrication of the SGFETs including lithographic process (spin-coating, multi-step optical lithography treatment, oxygen plasma discharge treatment), thermal evaporation of metals and encapsulation of transistor. The author characterized diamond samples (diamond grains, channels) by scanning electron microscope (SEM) and by optical microscope. The author participated in the designing and production of setup for measurement of transistor characteristics. The author participated in solving several technical issues such as encapsulation of SGFET, stability, cracking of covering resists, toxicity and biocompatibility and optimizing of measurement setup. The author measured transfer, output and gate current characteristics and participated on their evaluation and interpretation.

Bibliography

[1] J.M. Schakenraad, H.J. Busscher, Cell—polymer interactions: The influence of protein adsorption, Colloids Surf. 42 (1989) 331–343. doi:10.1016/0166-6622(89)80200-8.

[2] M.M. Browne, G.V. Lubarsky, M.R. Davidson, R.H. Bradley, Protein adsorption onto polystyrene surfaces studied by XPS and AFM, Surf. Sci. 553 (2004) 155–167. doi:10.1016/j.susc.2004.01.046.

[3] B. Rezek, E. Ukraintsev, L. Michalíková, A. Kromka, J. Zemek, M. Kalbacova, Adsorption of fetal bovine serum on H/O-terminated diamond studied by atomic force microscopy, Diam. Relat. Mater. 18 (2009) 918–922. doi:10.1016/j.diamond.2009.02.009.

[4] O. Babchenko, A. Kromka, K. Hruska, M. Kalbacova, A. Broz, M. Vanecek, Fabrication of nano-structured diamond films for SAOS-2 cell cultivation, Phys. Status Solidi A. 206 (2009) 2033–2037. doi:10.1002/pssa.200982215.

[5] M. Kalbacova, B. Rezek, V. Baresova, C. Wolf-Brandstetter, A. Kromka, Nanoscale topography of nanocrystalline diamonds promotes differentiation of osteoblasts, Acta Biomater. 5 (2009) 3076–3085. doi:10.1016/j.actbio.2009.04.020.

[6] A. Kromka, B. Rezek, M. Kalbacova, V. Baresova, J. Zemek, C. Konak, M. Vanecek, Diamond Seeding and Growth of Hierarchically Structured Films for Tissue Engineering, Adv. Eng. Mater. 11 (2009) B71–B76. doi:10.1002/adem.200800384.

[7] G. Zhao, O. Zinger, Z. Schwartz, M. Wieland, D. Landolt, B.D. Boyan, Osteoblast-like cells are sensitive to submicron-scale surface structure, Clin. Oral Implants Res. 17 (2006) 258–264. doi:10.1111/j.1600-0501.2005.01195.x.

[8] M. Tanaka, A. Takayama, E. Ito, H. Sunami, S. Yamamoto, M. Shimomura, Effect of pore size of self-organized honeycomb-patterned polymer films on spreading, focal adhesion, proliferation, and function of endothelial cells, J. Nanosci. Nanotechnol. 7 (2007) 763–772.

[9] M. Kalbacova, M. Kalbac, L. Dunsch, A. Kromka, M. Vaněček, B. Rezek, U. Hempel, S. Kmoch, The effect of SWCNT and nano-diamond films on human osteoblast cells, Phys. Status Solidi B. 244 (2007) 4356–4359. doi:10.1002/pssb.200776166.

[10] L. Tang, C. Tsai, W.W. Gerberich, L. Kruckeberg, D.R. Kania, Biocompatibility of chemical-vapour-deposited diamond, Biomaterials. 16 (1995) 483–488. doi:10.1016/0142-9612(95)98822-V.

[11] A. Kraft, Doped Diamond: A Compact Review on a New, Versatile Electrode Material, Int. J. Electrochem. Sci. 2007 (2007) 355–385.

[12] K.E. Toghill, R.G. Compton, Electrochemical non-enzymatic glucose sensors: a perspective and an evaluation, Int J Electrochem Sci. 5 (2010) 1246–1301.

[13] M.H. Abouzar, A. Poghossian, A. Razavi, A. Besmehn, N. Bijnens, O.A. Williams, K. Haenen, P. Wagner, M.J. Schöning, Penicillin detection with nanocrystalline-diamond field-effect sensor, Phys. Status Solidi A. 205 (2008) 2141–2145. doi:10.1002/pssa.200879713.

[14] B. Rezek, M. Krátká, A. Kromka, M. Kalbacova, Effects of protein inter-layers on cell–diamond FET characteristics, Biosens. Bioelectron. 26 (2010) 1307–1312. doi:10.1016/j.bios.2010.07.027.

[15]   M. Dankerl, S. Eick, B. Hofmann, M. Hauf, S. Ingebrandt, A. Offenhäusser, M. Stutzmann, J.A. Garrido, Diamond Transistor Array for Extracellular Recording From Electrogenic Cells, Adv. Funct. Mater. 19 (2009) 2915–2923. doi:10.1002/adfm.200900590.

[16]   W. Yang, O. Auciello, J.E. Butler, W. Cai, J.A. Carlisle, J.E. Gerbi, D.M. Gruen, T. Knickerbocker, T.L. Lasseter, J.N. Russell, L.M. Smith, R.J. Hamers, DNA-modified nanocrystalline diamond thin-films as stable, biologically active substrates, Nat. Mater. 1 (2002) 253–257. doi:10.1038/nmat779.

[17]   B. Rezek, D. Shin, H. Uetsuka, C.E. Nebel, Microscopic diagnostics of DNA molecules on mono-crystalline diamond, Phys. Status Solidi A. 204 (2007) 2827–2827. doi:10.1002/pssa.200790015.

[18]   M. Kalbacova, L. Michalikova, V. Baresova, A. Kromka, B. Rezek, S. Kmoch, Adhesion of osteoblasts on chemically patterned nanocrystalline diamonds, Phys. Status Solidi B. 245 (2008) 2124–2127. doi:10.1002/pssb.200879579.

[19]   B. Rezek, L. Michalíková, E. Ukraintsev, A. Kromka, M. Kalbacova, Micro-pattern guided adhesion of osteoblasts on diamond surfaces, Sensors. 9 (2009) 3549–3562. doi:10.3390/s90503549.

[20]   H. Kawarada, Hydrogen-terminated diamond surfaces and interfaces, Surf. Sci. Rep. 26 (1996) 205–206. doi:10.1016/S0167-5729(97)80002-7.

[21]   V. Chakrapani, J.C. Angus, A.B. Anderson, S.D. Wolter, B.R. Stoner, G.U. Sumanasekera, Charge transfer equilibria between diamond and an aqueous oxygen electrochemical redox couple, Science. 318 (2007) 1424–1430. doi:10.1126/science.1148841.

[22]   F. Maier, M. Riedel, B. Mantel, J. Ristein, L. Ley, Origin of Surface Conductivity in Diamond, Phys. Rev. Lett. 85 (2000) 3472–3475. doi:10.1103/PhysRevLett.85.3472.

[23]   C.E. Nebel, B. Rezek, D. Shin, H. Watanabe, T. Yamamoto, Electronic properties of H-terminated diamond in electrolyte solutions, J. Appl. Phys. 99 (2006) 033711. doi:10.1063/1.2171805.

[24]   B. Rezek, D. Shin, H. Watanabe, C.E. Nebel, Intrinsic hydrogen-terminated diamond as ion-sensitive field effect transistor, Sens. Actuators B Chem. 122 (2007) 596–599. doi:10.1016/j.snb.2006.07.004.

[25]   B. Rezek, E. Ukraintsev, A. Kromka, M. Ledinský, A. Brož, L. Nosková, H. Hartmannová, M. Kalbacova, Assembly of osteoblastic cell micro-arrays on diamond guided by protein pre-adsorption, Diam. Relat. Mater. 19 (2010) 153–157. doi:10.1016/j.diamond.2009.09.016.

[26]   G.T. Betzel, S.P. Lansley, F. Baluti, L. Reinisch, J. Meyer, Clinical investigations of a CVD diamond detector for radiotherapy dosimetry, Phys. Med. 28 (2012) 144–152. doi:10.1016/j.ejmp.2011.04.003.

[27]   D.M. Trucchi, E. Cappelli, N. Lisi, P. Ascarelli, Feasibility of CVD diamond radiation energy conversion devices, Diam. Relat. Mater. 15 (2006) 1980–1985. doi:10.1016/j.diamond.2006.08.012.

[28]   S. Spadaro, D.M. Trucchi, G. Conte, M. Pimpinella, A.S. Guerra, R.F. Laitano, Dynamic response of diamond sensors to ionizing radiation beams, Sens. Actuators Phys. 171 (2011) 43–47. doi:10.1016/j.sna.2010.12.017.

[29]   R.P. Hugtenburg, F.M. Saeedi, A.E.R. Baker, Determination of the energy response of closely tissue-equivalent diamond dosimeters for radiotherapy dosimetry, Appl. Radiat. Isot. 71 (2012) 23–24. doi:10.1016/j.apradiso.2012.03.016.

[30]   B. Planskoy, Evaluation of diamond radiation dosemeters, Phys. Med. Biol. 25 (1980) 519. doi:10.1088/0031-9155/25/3/011.

[31]   L. Grausova, L. Bacakova, A. Kromka, M. Vanecek, B. Rezek, V. Lisa, Molecular markers of adhesion, maturation and immune activation of human osteoblast-like MG 63 cells on nanocrystalline diamond films, Diam. Relat. Mater. 18 (2009) 258–263. doi:10.1016/j.diamond.2008.10.023.

[32]   E. Ukraintsev, B. Rezek, A. Kromka, A. Broz, M. Kalbacova, Long-term adsorption of fetal bovine serum on H/O-terminated diamond studied in situ by atomic force microscopy, Phys. Status Solidi B. 246 (2009) 2832–2835. doi:10.1002/pssb.200982257.

[33]   B. Alberts, D. Bray, A. Johnson, Essential Cell Biology, w. CD-ROM: An Introduction to the Molecular Biology of the Cell, Taylor & Francis, New York, 1997.

[34]   T. Ižák, V. Procházka, T. Sakata, B. Rezek, A. Kromka, Real-time Monitoring of Cell Activities by Diamond Solution-gated Field Effect Transistors, Procedia Eng. 168 (2016) 469–472. doi:10.1016/j.proeng.2016.11.130.

[35]   C.G. Specht, O.A. Williams, R.B. Jackman, R. Schoepfer, Ordered growth of neurons on diamond, Biomaterials. 25 (2004) 4073–4078. doi:10.1016/j.biomaterials.2003.11.006.

[36]   V. Procházka, M. Cifra, P. Kulha, T. Ižák, B. Rezek, A. Kromka, Influence of non-adherent yeast cells on electrical characteristics of diamond-based field-effect transistors, Appl. Surf. Sci. 395 (2017) 214–219. doi:10.1016/j.apsusc.2016.05.003.

[37]   M. Kalbacova, S. Roessler, U. Hempel, R. Tsaryk, K. Peters, D. Scharnweber, J.C. Kirkpatrick, P. Dieter, The effect of electrochemically simulated titanium cathodic corrosion products on ROS production and metabolic activity of osteoblasts and monocytes/macrophages, Biomaterials. 28 (2007) 3263–3272. doi:10.1016/j.biomaterials.2007.02.026.

[38]   B. Rezek, M. Krátká, E. Ukraintsev, O. Babchenko, A. Kromka, A. Brož, M. Kalbacova, Diamond as functional material for bioelectronics and biotechnology, in: New Perspect. Biosens. Technol. Appl., Intech, 2011: pp. 177–196.

[39]   L. Michalikova, B. Rezek, A. Kromka, M. Kalbacova, CVD diamond films with hydrophilic micro-patterns for self-organisation of human osteoblasts, Vacuum. 84 (2009) 61–64. doi:10.1016/j.vacuum.2009.04.016.

[40]   M. Varga, T. Izak, O. Rezek, M. Krátká, B. Rezek, A. Kromka, Intrinsic diamond as functional material for biosensor applications, in: Proc Sch. Vac. Technol. 2013, 2013: pp. 32–36.

[41]   T. Sakata, I. Makino, S. Kita, Real-time and noninvasive monitoring of respiration activity of fertilized ova using semiconductor-based biosensing devices, Eur. Biophys. J. EBJ. 40 (2011) 699–704. doi:10.1007/s00249-010-0653-4.

[42]   T. Ižák, K. Novotná, I. Kopová, L. Bačáková, B. Rezek, A. Kromka, H-terminated diamond as optically transparent impedance sensor for real-time monitoring of cell growth, Phys. Status Solidi B. 250 (2013) 2741–2746. doi:10.1002/pssb.201300098.

[43]   M. Krátká, N. Neykova, E. Ukraintsev, A. Kromka, B. Rezek, Sensitivity of encapsulated diamond-protein transistor renewed by low temperature hydrogen plasma, Int. J. Electrochem. Sci. 8 (2013) 1598–1608.

[44]   L.T. Hall, C.D. Hill, J.H. Cole, B. Städler, F. Caruso, P. Mulvaney, J. Wrachtrup, L.C.L. Hollenberg, Monitoring ion-channel function in real time through quantum decoherence, Proc. Natl. Acad. Sci. 107 (2010) 18777–18782. doi:10.1073/pnas.1002562107.

[45]   P.O. Bagnaninchi, N. Drummond, Real-time label-free monitoring of adipose-derived stem cell differentiation with electric cell-substrate impedance sensing, Proc. Natl. Acad. Sci. 108 (2011) 6462–6467. doi:10.1073/pnas.1018260108.

[46]   I. Giaever, C.R. Keese, A morphological biosensor for mammalian cells, Nature. 366 (1993) 591–592. doi:10.1038/366591a0.

[47]   I. Giaever, C.R. Keese, Monitoring fibroblast behavior in tissue culture with an applied electric field, Proc. Natl. Acad. Sci. 81 (1984) 3761–3764.

[48]   M. Dankerl, A. Reitinger, M. Stutzmann, J.A. Garrido, Resolving the controversy on the pH sensitivity of diamond surfaces, Phys. Status Solidi RRL – Rapid Res. Lett. 2 (2008) 31–33. doi:10.1002/pssr.200701266.

[49]   J. Doleček, Moderní učebnice elektroniky 2. díl, BEN - technická literatura, Praha, Czech Republic, 2005.

[50]   J. Vobecký, V. Záhlava, Elektronika součástky a obvody, principy a příklady, Grada Publishing, spol. s.r.o., Praha, 2001.

[51]   J.-P. Stengl, J. Tihanyi, Výkonové tranzistory MOSFET, BEN - technická literatura, Praha, Czech Republic, 1999.

[52]   MOSFET | Metal Oxide Semiconductor Field Effect Transistor | Electronics Notes. https://www.electronics-notes.com/articles/electronic_components/fet-field-effect-transistor/mosfet-metal-oxide-semiconductor-basics.php (accessed June 24, 2018).

[53]   MOSFET, Wikipedia. https://en.wikipedia.org/w/index.php?title=MOSFET&oldid=845359919 (accessed June 24, 2018).

[54]   MOSFET Characteristics. https://www.electrical4u.com/mosfet-characteristics/ (accessed June 24, 2018).

[55]   K.-S. Song, T. Hiraki, H. Umezawa, H. Kawarada, Miniaturized diamond field-effect transistors for application in biosensors in electrolyte solution, Appl. Phys. Lett. 90 (2007) 063901. doi:10.1063/1.2454390.

[56]   S. Ingebrandt, Y. Han, F. Nakamura, A. Poghossian, M.J. Schöning, A. Offenhäusser, Label-free detection of single nucleotide polymorphisms utilizing the differential transfer function of field-effect transistors, Biosens. Bioelectron. 22 (2007) 2834–2840. doi:10.1016/j.bios.2006.11.019.

[57]   C.E. Nebel, B. Rezek, D. Shin, H. Watanabe, T. Yamamoto, Electronic properties of H-terminated diamond in electrolyte solutions, J. Appl. Phys. 99 (2006) 033711. doi:10.1063/1.2171805.

[58]   K.-S. Song, G.-J. Zhang, Y. Nakamura, K. Furukawa, T. Hiraki, J.-H. Yang, T. Funatsu, I. Ohdomari, H. Kawarada, Label-free DNA sensors using ultrasensitive diamond field-effect transistors in solution, Phys. Rev. E. 74 (2006) 041919. doi:10.1103/PhysRevE.74.041919.

[59]   A. Härtl, B. Baur, M. Stutzmann, J.A. Garrido, Enzyme-Modified Field Effect Transistors Based on Surface-Conductive Single-Crystalline Diamond, Langmuir. 24 (2008) 9898–9906. doi:10.1021/la8014139.

[60]   A. Kromka, B. Rezek, Z. Remes, M. Michalka, M. Ledinsky, J. Zemek, J. Potmesil, M. Vanecek, Formation of Continuous Nanocrystalline Diamond

Layers on Glass and Silicon at Low Temperatures, Chem. Vap. Depos. 14 (2008) 181–186. doi:10.1002/cvde.200706662.

[61]   J. Čermák, A. Kromka, B. Rezek, Electrical characterization of locally charged oxidized nanocrystalline diamond films by Kelvin force microscopy, Phys. Status Solidi A. 205 (2008) 2136–2140. doi:10.1002/pssa.200879712.

[62]   A. Kromka, S. Potocky, B. Rezek, O. Babchenko, H. Kozak, M. Vanecek, M. Michalka, Role of polymers in CVD growth of nanocrystalline diamond films on foreign substrates, Phys. Status Solidi B. 246 (2009) 2654–2657. doi:10.1002/pssb.200982272.

[63]   K. Tsugawa, M. Ishihara, J. Kim, M. Hasegawa, Y. Koga, Large Area and Low Temperature Nanodiamond Coating by Microwave Plasma Chemical Vapor Deposition, New Diam. Front. Carbon Technol. 16 (2007) 337–346.

[64]   A. Kromka, O. Babchenko, T. Izak, K. Hruska, B. Rezek, Linear antenna microwave plasma CVD deposition of diamond films over large areas, Vacuum. 86 (2012) 776–779. doi:10.1016/j.vacuum.2011.07.008.

[65]   P. Hubík, J.J. Mareš, H. Kozak, A. Kromka, B. Rezek, J. Krištofik, D. Kindl, Transport properties of hydrogen-terminated nanocrystalline diamond films, Diam. Relat. Mater. 24 (2012) 63–68. doi:10.1016/j.diamond.2011.10.021.

[66]   Y. Sasaki, H. Kawarada, Low drift and small hysteresis characteristics of diamond electrolyte-solution-gate FET, J. Phys. Appl. Phys. 43 (2010) 374020. doi:10.1088/0022-3727/43/37/374020.

[67]   M. Krátká, A. Kromka, E. Ukraintsev, M. Ledinský, A. Brož, M. Kalbacova, B. Rezek, Function of thin film nanocrystalline diamond–protein SGFET independent of grain size, Sens. Actuators B Chem. 166–167 (2012) 239–245. doi:10.1016/j.snb.2012.02.049.

[68]   M. Krátká, A. Kromka, B. Rezek, A. Brož, M. Kalbacova, Characteristics of nanocrystalline diamond SGFETs under cell culture conditions, in: WDS11 Proc. Contrib. Pap. Part III Phys., MATFYZPRESS, Praha, Czech Republic, 2011: pp. 160–165.

[69]   H. Kozak, A. Kromka, M. Ledinsky, B. Rezek, Enhancing nanocrystalline diamond surface conductivity by deposition temperature and chemical post-processing, Phys. Status Solidi A. 206 (2009) 276–280. doi:10.1002/pssa.200824355.

[70]   O. Babchenko, T. Izak, E. Ukraintsev, K. Hruska, B. Rezek, A. Kromka, Toward surface-friendly treatment of seeding layer and selected-area diamond growth, Phys. Status Solidi B. 247 (2010) 3026–3029. doi:10.1002/pssb.201000124.

[71]   Scanning Electron Microscope - Radiological & Environmental Management - Purdue University. https://www.purdue.edu/ehps/rem/laboratory/equipment%20safety/Research%20 Equipment/sem.html (accessed June 6, 2018).

[72]   JEOL-JSM-6700F-SEM-Users-Manual, Handbook for users. JEOL, 2000.

[73]   I. Müllerová, Základy rastrovací elektronové mikroskopie, in: Brno, Czech Republic, 2003.

[74]   M. Ledinský, Optoelektronické a strukturní vlastnosti tenkých vrstev křemíku, PhD thesis, Charles University, 2009.

[75]   C.-C. Lin, M.-T. Kuo, H.-C. Chang, Review: Raman Spectroscopy–A Novel Tool for Noninvasive Analysis of Ocular Surface Fluid, J. Med. Biol. Eng. 30 (2010). doi:10.5405/jmbe.846.

[76]   J. Robertson, Diamond-like amorphous carbon, Mater. Sci. Eng. R Rep. 37 (2002) 129–281. doi:https://doi.org/10.1016/S0927-796X(02)00005-0.

[77]   A. Dychalska, P. Popielarski, W. Franków, K. Fabisiak, K. Paprocki, M. Szybowicz, Study of CVD diamond layers with amorphous carbon admixture by Raman scattering spectroscopy, Mater. Sci.-Pol. 33 (2015) 799–805. doi:10.1515/msp-2015-0067.

[78]   J. Čermák, Semiconductor - organic interface at nanoscale, PhD thesis, Charles University in Prague, 2010.

[79]   B. Rezek, H. Kozak, A. Kromka, Stabilizing diamond surface conductivity by phenol-formaldehyde and acrylate resins, Thin Solid Films. 517 (2009) 3738–3741. doi:10.1016/j.tsf.2009.02.126.

[80]   N. Neykova, O. Babchenko, H. Kozak, A. Kromka, K. Hruska, M. Vanecek, Novel route for hydrogen termination of nano - crystalline diamond films, in: Proc. 15th Int. Conf. Appl. Phys. Condens. Matter, Bystra, Liptovsky Jan, Slovak Republic, 2009: pp. 256–260.

[81]   N. Neykova, H. Kozak, M. Ledinsky, A. Kromka, Novel plasma treatment in linear antenna microwave PECVD system, Vacuum. 86 (2012) 603–607. doi:10.1016/j.vacuum.2011.07.055.

[82]   X.H. Li, C.T. Ha, D. Fu, M. Xiao, REDD1 Protects Osteoblast Cells from Gamma Radiation-Induced Premature Senescence, PLOS ONE. 7 (2012) e36604. doi:10.1371/journal.pone.0036604.

[83]   M. Krátká, O. Babchenko, E. Ukraintsev, J. Vachelová, M. Davídková, M. Vandrovcová, A. Kromka, B. Rezek, Gamma radiation effects on hydrogen-terminated nanocrystalline diamond bio-transistors, Diam. Relat. Mater. 63 (2016) 186–191. doi:10.1016/j.diamond.2015.10.015.

[84]   A. Kromka, O. Babchenko, T. Izak, M. Varga, M. Davydova, M. Kratka, B. Rezek, Diamond Films Deposited by Oxygen-Enhanced Linear Plasma Chemistry, Adv. Sci. Eng. Med. 5 (2013) 509–514. doi:10.1166/asem.2013.1331.

[85]   M. Geisler, T. Hugel, Aging of Hydrogenated and Oxidized Diamond, Adv. Mater. 22 (2010) 398–402. doi:10.1002/adma.200902198.

[86]   A. Poghossian, A. Cherstvy, S. Ingebrandt, A. Offenhäusser, M.J. Schöning, Possibilities and limitations of label-free detection of DNA hybridization with field-effect-based devices, Sens. Actuators B Chem. 111–112 (2005) 470–480. doi:10.1016/j.snb.2005.03.083.

[87]   P.K. Ang, K.P. Loh, T. Wohland, M. Nesladek, E. Van Hove, Supported Lipid Bilayer on Nanocrystalline Diamond: Dual Optical and Field-Effect Sensor for Membrane Disruption, Adv. Funct. Mater. 19 (2009) 109–116. doi:10.1002/adfm.200800770.

[88]   R. Hoffmann, A. Kriele, H. Obloh, N. Tokuda, W. Smirnov, N. Yang, C.E. Nebel, The creation of a biomimetic interface between boron-doped diamond and immobilized proteins, Biomaterials. 32 (2011) 7325–7332. doi:10.1016/j.biomaterials.2011.06.052.

[89]   T. Izak, M. Krátká, A. Kromka, B. Rezek, Osteoblastic cells trigger gate currents on nanocrystalline diamond transistor, Colloids Surf. B Biointerfaces. 129 (2015) 95–99. doi:10.1016/j.colsurfb.2015.03.035.

List of Abbreviations and Symbols

AFM – atomic force microscopy

BSA – bovine serum albumin

BSE – back-scattered electrons

CL – cathodoluminescence

CVD – chemical vapor deposition

DIW – deionized water

DNA – deoxyribonucleic acid

ECM – extracellular matrix

FBS – fetal bovine serum

FET – field-effect transistor

IDEs – interdigital electrodes

IGFET – insulated-gate field-effect transistor

JFET – junction field effect transistor

KFPM – Kelvin probe force microscopy

LAMPWP-CVD – linear antenna microwave plasma chemical vapor deposition

LTH – low temperature hydrogenation

MCD – monocrystalline diamond

MOSFET – metal-oxide- semiconductor field effect transistor

MWCVD – microwave plasma-enhanced chemical vapor deposition

NCD – nanocrystalline diamond

PBS – phosphate buffered saline

RIE – reactive ion etching

SE – secondary electrons

SEM – scanning electron microscopy

SGFET – solution-gated field-effect transistor

SPM – scanning probe microscopy

UDD – ultra-dispersed diamond

Symbols

Uds – drain-source voltage

Ut – threshold voltage

Ug – gate voltage

Udsat – saturation voltage

Ids – channel current

Igs – gate leakage current

g_m – transconductance

W – gate width

L – gate length

μ_n – charge-carrier effective mobility

C_{ox} – the gate oxide capacitance per unit area

λ – channel-length modulation parameter

About the author

Curriculum Vitae

Personal data

Name: Marie Krátká
Date of birth: February 1st 1982
Place of birth: Třebíč
Nationality: Czech
e-mail: kratka@fzu.cz

Education

2010 – present | Doctoral studies in the Faculty of Mathematics and Physics, Charles University in Prague, Czech Republic.
Study branch: Biophysics, chemical and macromolecular physics
PhD Thesis topic: Electronic effects at the interface between biomolecules, cells and diamond

(2012 – 2018 maternity leave)

August 2007 | Mgr. Degree obtained at Palacký University in Olomouc

2001 – 2007 | Graduated studies at the Faculty of Sciences, Palacký University in Olomouc, Czech Republic
Study branch: Biophysics
Mgr. Thesis topic: Absorption and emission of nanoparticles and nanocomposites based on iron oxides in visible region

Research interests

Preparation of solution gated field effect transistors (SGFETs) based on nanocrystalline diamond
Characterization SGFETs and their functionalization by proteins and cells
Scanning electron microscopy (SEM)

Languages

Czech, English, German (basic)

List of own publications and poster/oral presentations

Articles in reviewed journals and book chapter

1. B. Rezek, <u>M. Krátká</u>, A. Kromka, M. Kalbacova, **Effects of protein inter-layers on cell-diamond FET characteristics,** Biosens. Bioelectron. 26 (2010) 1307-1312

2. B. Rezek, E. Ukraintsev, <u>M. Krátká</u>, A. Kromka, A. Brož, M. Kalbáčová, **Biomedicínské aplikace diamantových vrstev,** Ces. Cas. Fyz., 61 (2011), 92-100

3. B. Rezek, <u>M. Krátká</u>, E. Ukraintsev, O. Babchenko, A. Kromka, A. Brož, M. Kalbacova, **Diamond as functional material for bioelectronics and biotechnology**
In: "New Perspectives in Biosensors Technology and Applications" Intech 2011, pp. 177-196, ISBN 978-953-307-448-1

4. <u>M. Krátká</u>, A. Kromka, E. Ukraintsev, M. Ledinský, A. Brož, M. Kalbačová, B. Rezek, **Function of thin film nanocrystalline diamond-protein SGFET independent of grain size**, Sensor Actuat. B-Chem. 166-167 (2012) 239 - 245

5. <u>M. Krátká</u>, N. Neykova, A. Kromka, B. Rezek, **Etching effects of low temperature hydrogen plasma on encapsulated diamond transistors**, Acta Universitatis Carolinae. Mathematica et Physica 53 (2012) 97-103

6. <u>M. Krátká</u>, N. Neykova, E. Ukraintsev, A. Kromka, B. Rezek, **Sensitivity of encapsulated diamond-protein transistor renewed by low temperature hydrogen plasma**, Int. J. Electrochem. Sci., 8 (2013) 1598-1608

7. Kromka, O. Babchenko, T. Izak, M. Varga, M. Davydova, <u>M. Krátká</u>, B. Rezek, **Diamond Films Deposited by Oxygen-Enhanced Linear Plasma Chemistry**, Adv. Sci. Eng. Med. 5 (2013) 509-514

8. Rezek, E. Ukraintsev, <u>M. Krátká</u>, A. Taylor, F. Fendrych, V. Mandys, **Epithelial cells morphology and adhesion on diamonds films deposited and chemically modified by plasma processes**, Biointerphases 9 (2014) 031012 (1)-031012(8)

9. T. Izak, <u>M. Krátká</u>, A. Kromka, B. Rezek, **Osteoblastic cells trigger gate currents on nanocrystalline diamond transistor**. Colloid Surf. B-Biointerfaces 129 (2015) 95 - 99.

10. <u>M. Krátká</u>, O. Babchenko, E. Ukraintsev, J. Vachelová, M. Davídková, M. Vandrovcová, A. Kromka, B. Rezek. **Gamma radiation effects on hydrogen-terminated nanocrystalline diamond bio-transistors**. Diam. Relat. Mater. 63 (2016) 186 - 191.

Conference proceedings

1. <u>M. Krátká</u>, A. Kromka, E. Ukraintsev, A. Brož, M. Kalbáčová, B. Rezek, **Nanocrystalline diamond SG-FET: role of grain boundaries and cell culture process,** Proceedings of the International Workshop on Diamond Nanotechnology and Science Progress – DINAS, 2011

2. <u>M. Krátká</u>, A. Kromka, A. Brož, M. Kalbáčová, B. Rezek, **Characteristics of nanocrystalline diamond SGFETs under cell culture conditions**, Proc. of the 20th Annual Conference of Doctoral Students - WDS 2011, Part III, 160–165, 2011, ISBN 978-80-7378-186-6, 2011

3. <u>M. Krátká</u>, N. Neykova, E. Ukraintsev, A. Kromka, B. Rezek, **Renewal of three-dimensional nanocrystalline diamond bio-transistor by low temperature hydrogenation**, Proc. of the XII. Workshop of Physical Chemists and Electrochemists 2012, 110-112, ISBN 978-80-7375-618-5

4. M. Varga, T. Izak, O. Rezek, <u>M. Krátká</u>, B. Rezek, A. Kromka, **Intrinsic diamond as functional material for biosensor applications**, Proc. of the School of Vacuum Technology 2013, 32-36, ISBN 978-80-971179-2-4

5. Rezek, E. Ukraintsev, <u>M. Krátká</u>, A. Taylor, F. Fendrych, V. Mandys, **Microscopic morphology of epithelial cells on functionalized diamond and glass**, Proc. of the 6th Conference on Solid State Surfaces and Interfaces 2013, 153-154, ISBN 978-80-223-3501-0

Conference contributions and presentations

1. <u>M. Krátká</u>, B. Rezek, J. Čermák, M. Ledinský, A. Kromka, A. Brož, M. Kalbáčová, **Protein adsorption and cell growth cause permanent gate potential shifts of H-diamond SGFETs**, oral presentation at E-MRS Spring Meeting, 2010, Strasbourg, France

2. B. Rezek, E. Ukraintsev, <u>M. Krátká</u>, A. Kromka, M. Kalbacova, **Effects of protein inter-layers on cell-diamond FET characteristics**, poster presentation at 20th Anniversary World Congress on Biosensors, 2010, Glasgow, UK

3. <u>M. Krátká</u>, B. Rezek, J. Čermák, M. Ledinský, A. Kromka, A. Brož, M. Kalbacova, **Protein adsorption and cell growth cause permanent gate**

potential shifts of H-diamond SGFETs, oral presentation for the bilateral project between ASCR and Uppsala University, 2010

4. <u>M. Krátká</u>, A. Kromka, A. Brož, M. Kalbacova, B. Rezek: **Characteristics of nanocrystalline diamond SGFETs under cell culture conditions**, oral presentation at 20th Annual Student Conference (WDS 2011), 2011, Prague, Czech Republic

5. <u>M. Krátká</u>, O. Babchenko, E. Ukraintsev, A. Kromka, B. Rezek, **Three-dimensional nanocrystalline diamond bio-transistor**, oral presentation at 22nd European Conference on Diamond, Diamond-Like Materials, Carbon Nanotubes and Nitrides, 2011, Garmish-Partenkirchen, Germany

6. <u>M. Krátká</u>, A. Kromka, A. Brož, M. Kalbáčová, B. Rezek, **Influence of proteins and cell culturing process on nanocrystalline diamond SGFET characteristics**, poster presentation at 22nd European Conference on Diamond, Diamond-Like Materials, Carbon Nanotubes and Nitrides, 2011, Garmish-Partenkirchen, Germany

7. Kromka, O. Babchenko, <u>M. Krátká</u>, B. Rezek, **Electrical conductivity of nanodiamond films deposited by oxygen-enhanced linear plasma chemistry**, presentation at 25th International Winterschool On Electronic Properties Of Novel Materials - IWEPNM 2011, February 26 - March 05, 2011, Kirchberg, Austria

8. <u>M. Krátká</u>, A. Kromka, E. Ukraintsev, A. Brož, M. Kalbáčová, B. Rezek, **Nanocrystalline diamond SG-FET: role of grain boundaries and cell culture process**, poster presentation at International Workshop on Diamond Nanotechnology and Science Progress – DINAS, 2011, Prague, Czech Republic

9. <u>M. Krátká</u>, A. Kromka, A. Brož, M. Kalbáčová, B. Rezek**, Elektronické jevy na rozhraní biomolekul, buněk a diamantu**, oral presentation at seminar in Nová Paka, 2011, Nová Paka, Czech Republic

10. <u>M. Krátká</u>, N. Neykova, E. Ukraintsev, A. Kromka, B. Rezek, **Renewal of three-dimensional nanocrystalline diamond bio-transistor by low temperature hydrogenation**, poster presentation at XII. Workshop of Physical Chemists and Electrochemists, 2012, Brno, Czech Republic

11. <u>M. Krátká</u>, N. Neykova, A. Kromka, B. Rezek, **Etching effects of low temperature hydrogen plasma on encapsulated diamond transistors**, oral presentation at 21st Annual Conference of Doctoral Students, 2012, Prague, Czech Republic

12. <u>M. Krátká</u>, A. Kromka and B. Rezek, **Cell-protein field-effect transistors based on nanocrystalline diamond**, oral presentation at Summer School and Workshop on Biomaterials and Regenerative Medicine, 2012, Riva del Garda, Italy

13. Kromka, O. Babchenko, T. Izak, M. Varga, M. Davydova, <u>M. Krátká</u>, B. Rezek, **Diamond Films Deposited by Oxygen-Enhanced Linear Plasma Chemistry**, oral presentation at Development of Materials Science in Research and Education, 2012, Lednice, Czech Republic

14. Rezek, E. Ukraintsev, J. Čermák, <u>M. Krátká</u>, A. Kromka, **Characterization of physisorption and chemisorption of molecules on diamond by scanning probe measurements**, poster presentation at E-MRS 2012 Fall Meeting, 2012, Warsaw, Poland

15. T. Izak, <u>M. Krátká</u>, A. Kromka, B. Rezek, **Effect of osteoblastic cells on function of nanocrystalline diamond transistors**, presentation at 3rd International Conference on Materials and Applications for Sensors and Transducers (ICMAST), 2013, Prague, Czech Republic

16. E. Ukraintsev, B. Rezek, <u>M. Krátká</u>, A. Taylor, F. Fendrych, V. Mandys, **Epithelial cell morphology and adhesion on diamond films grown by linear antenna MW-PECVD**, presentation at Hasselt Diamond Workshop 2013 - SBDD XVIII, 2013, Hasselt, Belgium

17. T. Itoh, A. Vetushka, Y. Nakanishi, <u>M. Krátká</u>, M. Ledinský, A. Fejfar, S. Nonomura, J. Kočka. **Local Structure and Electrical Properties of Carbon Nanowalls**. Ooyo butsuri gakkai (Japanese Applied Physics Conference)

18. <u>M. Krátká</u>, O. Babchenko, E. Ukraintsev, J. Vachelová, M. Davídková, M. Vandrovcová, A. Kromka, B. Rezek. **Gamma radiation effects on H-diamond bio-transistors.** Abstract book, 9th International Conference on New Diamond and Nano Carbon (NDNC), 24th-29th May 2015, Shizuoka, Japan

Attached author´s representative publications

1. B. Rezek, M. Krátká, A. Kromka, M. Kalbacova. Effects of protein interlayers on cell-diamond FET characteristics. Biosens. Bioelectron. 26 (2010) 1307 - 1312.

2. M. Krátká, A. Kromka, E. Ukraintsev, M. Ledinský, A. Brož, M. Kalbačová, B. Rezek. Function of thin film nanocrystalline diamond-protein SGFET independent of grain size. Sensor Actuat. B-Chem. 166-167 (2012) 239 - 245.

3. Marie Krátká, Neda Neykova, Egor Ukraintsev, Alexander Kromka, Bohuslav Rezek. Sensitivity of encapsulated diamond-protein transistor renewed by low temperature hydrogen plasma. Int. J. Electrochem. Sci. 8 (2013) 1598 - 1608.

4. T. Izak, M. Krátká, A. Kromka, B. Rezek. Osteoblastic cells trigger gate currents on nanocrystalline diamond transistor. Colloid Surf. B-Biointerfaces 129 (2015) 95 - 99.

5. M. Krátká, O. Babchenko, E. Ukraintsev, J. Vachelová, M. Davídková, M. Vandrovcová, A. Kromka, B. Rezek. Gamma radiation effects on hydrogen-terminated nanocrystalline diamond bio-transistors. Diam. Relat. Mater. 63 (2016) 186 - 191.